KURIHARA
INTERNATIONAL PATENT OFFICE
PATENT ATTORNEYS

IWASAKI BLDG. 7F,
3-15, HIROO 1-CHOME,
SHIBUYA-KU, TOKYO 150-0012
JAPAN
TELEPHONE : 81-3-3444-6361
FACSIMILE : 81-3-3444-6362

VIA TELEFAX (42 page(s))-CONFIRMATION MAIL

December 19, 2005

Mr. Donald W. Huntley
HUNTLEY & ASSOCIATES
1105 NORTH MARKET STREET
P.O.BOX 948
WILMINGTON DE 19899-0948
U. S. A.

Re: Your Ref.: Hokushin-6(13341)
Our Ref.:FP20030801US
Title: Moderately Resistive Rubber Composition and Rubber Member
U.S. Patent Application Serial No. 10/734,021
Due date: January 4, 2006

Dear Mr. Huntley,

Thank you for your letter of October 12, 2005.

We would like to respond to the office Action dated October 4, 2005 in accordance with the attached our comments.

Please be informed that our office will close from December 29, 2005 to January 4, 2006. If you have any questions please contact us before December 26, 2005.

Thank you for your help.

Very truly yours,

Hiroyuki Kurihara

HK/rm
Enlc.

1. With respect to "ionic liquid"

The term "ionic liquid" is the general terms (shown in References 1 to 5 as attached).

<Reference 1>
Masahiro Yoshizawa, Wataru Ogihara, and Hiroyuki Ohno, "Novel Polymer Electrolytes Prepared by Copolymerization of Ionic Liquid Monomers", Polymers for Advanced Technologies, 13, p.589-594 (2002)
<Reference 2>
Masafumi Yoshio, Tomohiro Mukai, Kiyoshi Kanie, Masahiro Yoshizawa, Hiroyuki Ohno, and Takashi Kato, "Liquid-Crystalline Assemblies Containing Ionic Liquids: An Approach to Anisotropic Ionic Materials", Chemistry Letters p.320-321 (2002)
<Reference 3>
Ann E. Visser, W. Matthew Reichert, Richard P. Swatloski, Heather D. Willauer, Jonathan G. Huddleston, and Robin D. Rogers, "Characterization of Hydrophilic and Hydrophobic Ionic Liquids: Alternatives to Volatile Organic Compounds for Liquid-Liquid Separations", ACS Symposium Series (American Chemical Society), p.289-308 (2002)
<Reference 4>
Masayoshi Watanabe, Tomoo Mizumura, "Conductivity study on ionic liquid/polymer complexes", Solid state Ionics, p.353-356 (1996)
<Reference 5>
Timothy I. Morrow and Edward J. Maginn, "Molecular Dynamics Study of the Ionic Liquid 1-*n*-Butyl-3-methylimidazolium Hexafluorophosphate", Journal of Physical Chemistry B, 106, p.12807-12813 (2002)

The term "ionic liquid" refers to a salt which is in the liquid state at room temperature (may be called "ambient temperature molten salt"), and particularly to a salt having a melting point of 70°C or less, preferably 30°C or less. Such an ionic liquid has no vapor pressure (non-volatility), exhibits high thermal resistance and

MUTUAL NON-DISCLOSURE AGREEMENT

This Mutual Non-Disclosure Agreement ("Agreement") effective as of the last date of the signatures hereto (the "Effective Date") between RF Micro Devices, Inc. and its wholly owned subsidiaries ("RFMD"), a corporation having its principal place of business at 7628 Thorndike Road, Greensboro, North Carolina 27409, and Diemat Incorporated, a corporation having its principal place of business at 19 Central Street, Byfield, MA 01922 ("PARTICIPANT") (individually a "Party" and collectively the "Parties").

WHEREAS, the Parties desire to enter into discussions regarding *technology for mixing of ferrite paste and its potential applications* (the "Purpose"); and

WHEREAS, the Parties desire to disclose certain Confidential Information (as defined below) on a confidential basis to further the Purpose.

NOW THEREFORE, in consideration of the disclosure of Confidential Information by either Party, the Parties agree as follows:

1. Definitions:

a. The Party receiving Confidential Information from the other Party shall be the "Receiving Party" and the Party disclosing Confidential Information to the other Party shall be the "Disclosing Party."

b. "Confidential Information" shall mean any information or data, whether owned by a Party or its Affiliates or obtained from a third party subject to a confidential arrangement, including, but not limited to, "Trade Secret Information" and "Business Information," disclosed by one Party to the other, in connection with the Purpose, irrespective of the medium in which such information or data is embedded, which information if in tangible or electronic form is marked as proprietary or confidential by the Disclosing Party, is designated by the Disclosing Party as being confidential at the time of such disclosure, or which under the circumstances surrounding the disclosure gives the indicia that the information should be treated as confidential. Confidential Information shall include any copies or abstracts made thereof as well as any modules, samples, prototypes, or parts thereof embodying such Confidential Information.

c. "Trade Secret Information" includes, but is not limited to, product specifications, data, technical know-how, formulae, processes, designs, sketches, photographs, graphs, drawings, samples, prototypes, inventions and ideas, past, current, and planned research and development, current and planned manufacturing methods and processes, computer software and programs (including object code and source code), draft or pending patent applications, and other similar technical materials, however documented.

d. "Business Information" includes, but is not limited to, information concerning the business and affairs of the Disclosing Party, which may include unpublished financial projections and budgets, projected sales, capital spending budgets and plans, personnel information of the Disclosing Party, marketing plans, and other business information.

e. "Affiliate" shall mean any company or other entity of which, and as long as, at least fifty percent (50%) of the outstanding shares or securities representing the right to vote for the election of directors or other managing authority are, now or hereafter, directly or indirectly owned by a Party.

2. Confidential Information of the Disclosing Party shall remain the property of the Disclosing Party. The Receiving Party agrees to protect the Confidential Information of the Disclosing Party against unauthorized disclosure with at a minimum the same degree of care as it applies to its own confidential information of like nature, but in no event less than a reasonable degree of care and warrants that it has in place reasonable safeguards against the unauthorized disclosure of Confidential Information.

3. The Confidential Information provided by the Disclosing Party to the Receiving Party shall not be used by Receiving Party to prepare any patent application or to provoke any interference with any patent application that has been or may be filed on behalf of the Disclosing Party, including any continuing and/or divisional patent application that has been or may be filed. The Confidential Information of the Disclosing Party shall not be used by the Receiving Party

incombustibility, and is chemically stable (shown in p.6 lines 12-19 of the present specification). Accordingly "ionic liquid" does not refer to a state of matter which dependent upon conditions but refers to specific compounds. Consequently "ionic liquid" does not mean the ionic compounds in the liquid form.

Therefore, we believe that the term "ionic liquid" in claims 1 to 6 is appropriate.

2. With respect to Claim Rejections - 35 USC § 102

Angell(USP5962169) discloses the rubbery materials(column 5 line 22-23 etc.). That is to say, ionic liquid is rubbery itself in Angell (column 3 lines 16-18). On the other hand, the present invention is the rubber with ionic liquid. Therefore, the present invention is different from Angell.

3. With respect to Claim Rejections - 35 USC § 103

Kitano(USP6810225) discloses ionic compounds, but does not disclose the compounds corresponding to the ionic liquid. On the other hand, the present invention uses the "ionic liquid".

Takashima(USP6458883) also does not disclose the compounds corresponding to the ionic liquid.

Angell also does not disclose the compounds corresponding to the ionic liquid.

Michot(USP6841304) disclose molten salts and the molten salts are used in electrolytic solutes(Title), but does not disclose that the molten salts are added to a rubber. Accordingly, the technical field of Michot is different from the technical field of the present invention related to rubber composition and rubber member.

Therefore, the present invention is not obvious from Kitano, Takashima, Michot and Angell.

POLYMERS FOR ADVANCED TECHNOLOGIES
Polym. Adv. Technol. 13, 589–594 (2002)
Published online in Wiley InterScience (www.interscience.wiley.com). DOI:10.1002/pat.261

Novel Polymer Electrolytes Prepared by Copolymerization of Ionic Liquid Monomers

Masahiro Yoshizawa, Wataru Ogihara and Hiroyuki Ohno*

Department of Biotechnology, Tokyo University of Agriculture and Technology, Koganei, Tokyo 184-8588, Japan

ABSTRACT

Ionic liquid monomer couples were prepared by the neutralization of 1-vinylimidazole with vinylsulfonic acid or 3-sulfopropyl acrylate. These ionic liquid monomer couples were viscous liquid at room temperature and showed low glass transition temperature (Tg) at −83°C and −73°C, respectively. These monomer couples were copolymerized to prepare ion conductive polymer matrix. Thus prepared ionic liquid copolymers had no carrier ions, and they showed very low ionic conductivity of below 10^{-9} S cm^{-1}. Equimolar amount of lithium bis(trifluoromethanesulfonyl)imide (LiTFSI) to imidazolium salt unit was then added to generate carrier ions in the ionic liquid copolymers. Poly(vinylimidazolium-co-vinylsulfonate) containing equimolar LiTFSI showed the ionic conductivity of 4×10^{-9} S cm^{-1} at 30°C. Advanced copolymer, poly(vinylimidazolium-co-3-sulfopropyl acrylate) which has flexible spacer between the anionic charge and polymer main chain, showed the ionic conductivity of about 10^{-6} S cm^{-1} at 30°C, which is 100 times higher than that of copolymer without spacer. Even an excess amount of LiTFSI was added, the ionic conductivity of the copolymer kept this conductivity. This tendency is completely different from the typical polyether systems. Copyright © 2002 John Wiley & Sons, Ltd.

*Correspondence to: H. Ohno, Department of Biotechnology, Tokyo University of Agriculture and Technology, Koganei, Tokyo 184-8588, Japan.
E-mail: ohnoh@cc.tuat.ac.jp

KEYWORDS: Ionic liquid; Molten salt; Ionic conductivity; Glass transition temperature; Solid polymer electrolyte

INTRODUCTION

Recently, air- and water-stable ionic liquids have been prepared by the combination of imidazolium cation and specific organic anions [1, 2]. Since these ionic liquids are composed of only ions, they have very high carrier ion concentration and accordingly show high ionic conductivity at room temperature [3–7]. Furthermore, ionic liquids are widely spread as some kinds of reaction media and extraction solvent, because of very unique properties, such as nonvolatility, low viscosity, and immiscible with water when fluorine-rich anions were used [8–11].

Since ionic liquids are empirically known to be prepared with imidazolium salts, several imidazolium cation derivatives are used to form ionic liquids [12]. The ionic liquids are generally prepared through the anion exchange process from salts having halide anions. There are some drawbacks such as incomplete anion exchange process and contamination of by-products. In addition, this method is limited for only several anion species. Development of new ionic liquids is not so rapid, in spite of unlimited combination of cations and anions [1–7].

We then proposed novel synthesis method to prepare ionic liquid by the neutralization of the tertiary amines with acids [13, 14]. This method is

Received 5 November 2001
Accepted 13 March 2002

useful for not only the improvement of the synthesis but also the analysis of the relation between ionic liquid structure and their properties (glass transition temperature, melting point, viscosity, ionic conductivity, and so on). This neutralization method is capable to prepare desired ionic liquid from one pot reaction without any by-product. We discussed the effect of counter anions on the properties of ionic liquid by changing acid species [14]. Ionic liquids thus prepared by the neutralization method are suitable as model compounds for dialkylimidazolium salts. Several important factors of amines and acids were obtained to design excellent ionic liquids.

Since ionic liquids show excellent ionic conductivity, they are also investigated as a component of an electrolyte matrix. Especially, the developments of polymer gel electrolytes have been carried out with polymers containing ionic liquids [15–17]. However, ordinary ionic liquids are improper as an electrolyte, because component ions of ionic liquid migrate along with the potential gradient. This is a fetal drawback when only target ions such as lithium cations are aimed to be transported.

We have reported two methods to solve such a problem. One is the zwitterionic-type ionic liquid, of which both cation and counter anion were tethered [18]. The other is the ionic liquid polymer, in which cations or counter anions were attached on the vinyl polymer [19]. Although zwitterionic-type ionic liquids have relatively high Tm, lithium transference numbers in these zwitterionic-type ionic liquids exceed 0.5. Such a matrix should be suitable for target ion transport when the ion migration was accelerated. On the other hand, we have designed ionic liquid polymers such as polycation [20, 21], polycation-type polymer brush [22, 23], and polyanion [24, 25]. These are obtained by the polymerization of ionic liquid monomers, which have vinyl groups on either cations or counter anions. In addition, polymerization of ionic liquid is effective to not only transport target ions selectively but also generate carrier ions. It is widely known that cationic and anionic polymers offer an atmosphere with high dielectric constant, which facilitates the dissociation of lithium salts in the matrix [26]. However, polymerization of ionic liquid components induced considerable decrease in the mobility of ions in the matrix due to the increase of glass transition temperature. So far, it is necessary to increase mobility of ionic liquid structure by introducing spacer between polymer main chain and salt structure [22, 23].

In this paper, we introduced vinyl groups in both cation and anion, and novel ionic liquid polymers were prepared by the copolymerization of these ionic liquid monomers.

EXPERIMENTAL

Materials

1-Vinylimidazole and 3-sulfopropyl acrylate potassium salt were purchased from Aldrich Chemical Co. Sodium vinylsulfonate was purchased from Kanto Chemical Co. Inc. These were used as received. α,α'-Azobis(isobutyronitrile) (AIBN) was recrystallized from methanol before use.

Lithium bis(trifluoromethanesulfonyl)imide (Li TESI) was a gift from Sumitomo 3M corporation.

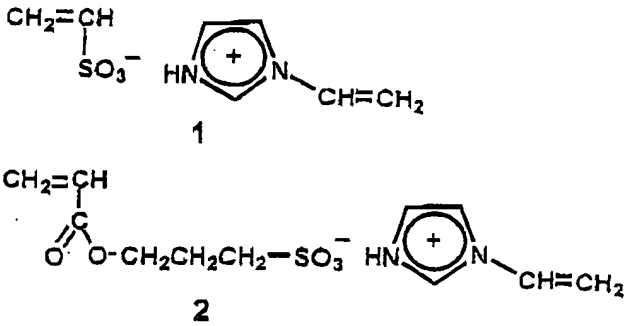

SCHEME 1. Structure of ionic liquid monomers obtained by neutralization.

Synthesis of ionic liquid monomers

Alkali metal cations of sodium vinylsulfonate and 3-sulfopropyl acrylate potassium salt were substituted into proton by means of cation exchange resin (Amberlite IR-120B H AG). Aqueous solutions of these acids were slowly mixed with equimolar amount of 1-vinylimidazole on ice bath. The mixture was stirred at room temperature for a day. The aqueous solution was then dried with a rotary evaporator; the residual viscous liquid was pored into dehydrated diethyl ether and stirred for 1 hour. The viscous liquid was collected and dried. This was repeated twice and the obtained salt was dried *in vacuo* at room temperature. The structure of the obtained ionic liquid monomers as shown in Scheme 1 was confirmed with ^{1}H-NMR.

Polymerization of ionic liquid monomers

Radical polymerization of these monomers was initiated with AIBN (1 mol%) in ethanol at 60 °C under N_2 atmosphere. After polymerization, the solution was poured into a large excess acetone. Precipitation was washed with dehydrated methanol and dried *in vacuo* at 60 °C.

Methods

The structure of these ionic liquid monomers was confirmed by ^{1}H-NMR spectroscopy (JEOL α-500 NMR spectrometer).

The ionic conductivity of the obtained compounds was measured with the complex-impedance method using an impedance analyzer (Schlumberger Solartron 1260 impedance/gain-phase analyzer) with a frequency range from 10 Hz to 5 MHz. The dynamic ionic conductivity measurement system was developed in our laboratory [27]. All measurements were carried out in a

TABLE 1. Effect of polymerization time on the ionic conductivity and Tg

	Polymerization Time (h)	Tg (°C)	σ_i at 30°C (S cm^{-1})	State
1	Monomer	−83	3.5×10^{-3}	Liquid
P1a	3	−75	8.5×10^{-5}	Rubber-like
P1b	6	—	$<10^{-9}$	Solid
P1c	12	—	$<10^{-9}$	Solid
P1	24	—	$<10^{-9}$	Solid

—; not detected

globe box under dry N_2 atmosphere in the temperature range 10°C to 60°C at a cooling rate of 2.5°C min^{-1}.

DSC measurement was carried out with a DSC-6200 (Seiko Instruments Inc.) in the temperature range −150°C to 200°C at a heating rate of 10°C min^{-1}.

RESULTS AND DISCUSSION

Ionic liquid monomer 1 was obtained as a yellow transparent viscous liquid at room temperature. It is known that imidazolium salts with fluorinated anions, like BF_4^-, $CF_3SO_3^-$, and $TFSI^-$, form excellent ionic liquid [6]. The monomer 1 was obtained as liquid with Tg of −83°C. Viscosity of 1, however, exceeds 1000 cP at room temperature, which is much higher than that for other typical ionic liquids. In spite of high viscosity, 1 showed relatively high ionic conductivity of 3.5×10^{-3} S cm^{-1} at room temperature reflecting low Tg.

Ionic liquid copolymer P1 (P implies polymer) has been prepared by copolymerization of ionic liquid monomer 1. Table 1 summarizes the effect of polymerization time on the ionic conductivity and Tg for 1. When polymerization time was 3 hours, rubber-like polymer P1a with Tg of −75°C was obtained. Only when the polymerization time exceeded 6 hours, polymerized 1 became solid or powder. An obvious Tg for these polymers cannot be detected with DSC apparatus used in our experiments.

Since the copolymers have no carrier ions because both cations and anions were fixed on polymer main chain, they should show very poor ionic conductivity. P1a showed relatively high ionic conductivity of 8.5×10^{-5} S cm^{-1} at 30°C. This can be comprehended to be due to low molecular weight matrix, like oligomer. On the other hand, the ionic conductivity of P1b, P1c, and P1, which were prepared by longer polymerization time (> 6 hours), was less than 10^{-9} S cm^{-1} at 30°C. Although the molecular weight of P1 was not measured yet, improved average molecular weight was confirmed as the decrease of the ionic conductivity. Unless otherwise stated, polymerization time of P1 is 24 hours hereafter.

In order to characterize P1 as an ion conductive matrix, three kinds of lithium salts ($LiBF_4$, $LiCF_3SO_3$, and LiTFSI) were added equimolarly to imidazolium salt unit of P1. Fig. 1 shows temperature dependence of the ionic conductivity for P1 containing equimolar amount of lithium salt. P1 with LiTFSI showed ionic conductivity of 7.2×10^{-7} S cm^{-1} at 50°C, whereas that of P1 with $LiCF_3SO_3$ or $LiBF_4$ was only 10^{-9} S cm^{-1}. This considerable increase in the ionic conductivity by the addition of LiTFSI cannot be explained only by higher degree of dissociation of the added salt. $TFSI^-$ is known to act as a plasticizer [28], and this was also confirmed in the case of this copolymer. However DSC measurements were performed for these samples, their Tg was not detected clearly. The lowering of Tg cannot be confirmed with the DSC measurement, but the increase of the ionic

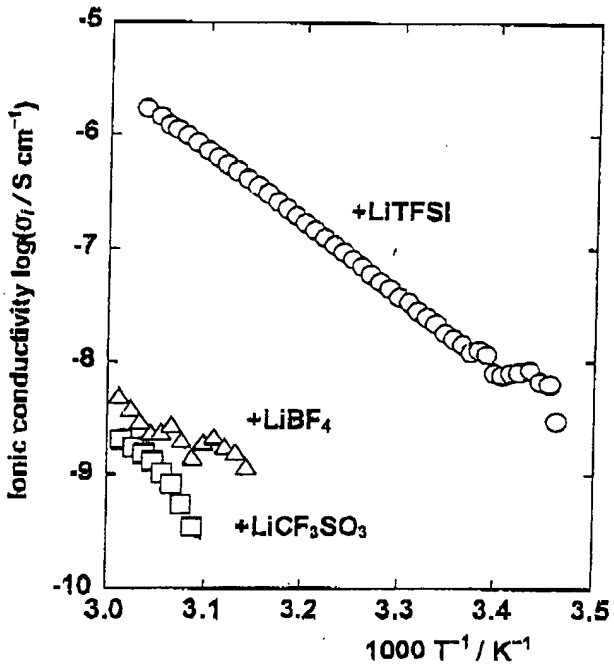

FIGURE 1. Temperature dependence of the ionic conductivity for P1 containing LiX (X = BF_4^-, $CF_3SO_3^-$, $TFSI^-$). [LiX]/[Im^+] = 1.0 (by mol ratio)

TABLE 2. The ionic conductivity at room temperature and Tg of each monomers and their copolymers

	Tg (°C)		σ_i (S cm^{-1})	
	Monomer	Polymer	Monomer	Polymer
1	−83	—	3.5×10^{-3}	$<10^{-9}$
2	−73	−31	6.5×10^{-4}	$<10^{-9}$

—: not detected
Polymers were obtained by the copolymerization of corresponding monomers for 24 hours.

conductivity clearly indicated it. Similar tendency was reported on the zwitterionic-type ionic liquids [18].

However P1, mixed with equimolar amount of LiTFSI, showed the highest ionic conductivity among three, this needs further improvement on the ionic conductivity. For this, we designed new ionic liquid copolymer, which have flexible spacer between vinyl group and counter anion structure expecting higher segmental motion. In our previous study, comb-shaped polymers were analyzed, and introduction of spacer between polymer main chain and cation charge was revealed to be effective to maintain high ionic conductivity even after polymerization [22, 23]. Table 2 shows Tg and the ionic conductivity of ionic liquid monomers 1, 2, and corresponding their copolymers. Compound 2 is liquid at room temperature as well as 1 and shows the Tg at −73 °C. In spite of low Tg, the ionic conductivity of 2 was 6.5×10^{-4} S cm^{-1} at room temperature, which is one order lower than that of 1. We considered that larger anion structure of ionic liquid monomer 2 leads to lower ionic conductivity. After polymerization for 24 hours, P2 showed very low ionic conductivity (less than 10^{-9} S cm^{-1}) similarly to that of P1. P1 showed no Tg at the temperature range for this measurement, whereas P2 showed relatively low Tg of −31 °C. From these, P2 containing lithium salt was expected to show higher ionic conductivity than that of P1.

Equimolar amount of LiTFSI was also added to P2 to compare the ionic conductivity. P2 containing equimolar LiTFSI showed the ionic conductivity of 1.2×10^{-6} S cm^{-1} at 30 °C, which was 30 times higher than that of P1 as shown in Fig.2. This difference is attributed to the following two factors:

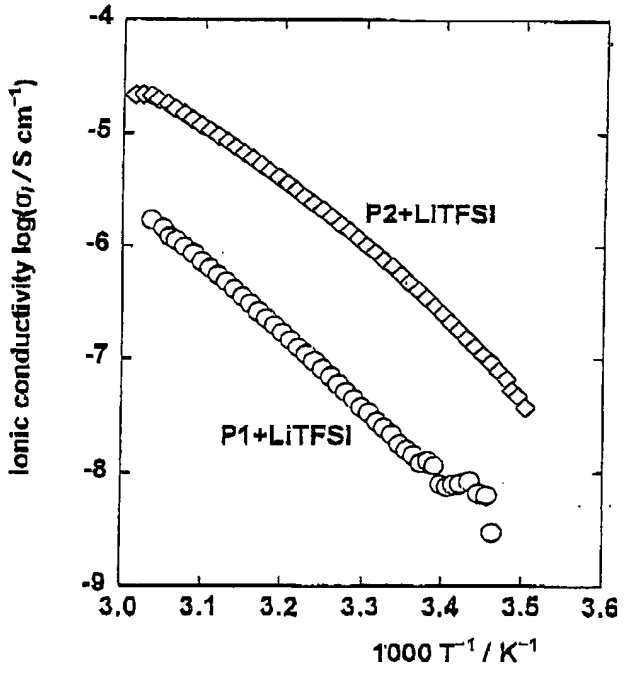

FIGURE 2. Temperature dependence of the ionic conductivity for P1 and P2 containing LiTFSI. [LiTFSI]/[Im$^+$] = 1.0 (by mol ratio)

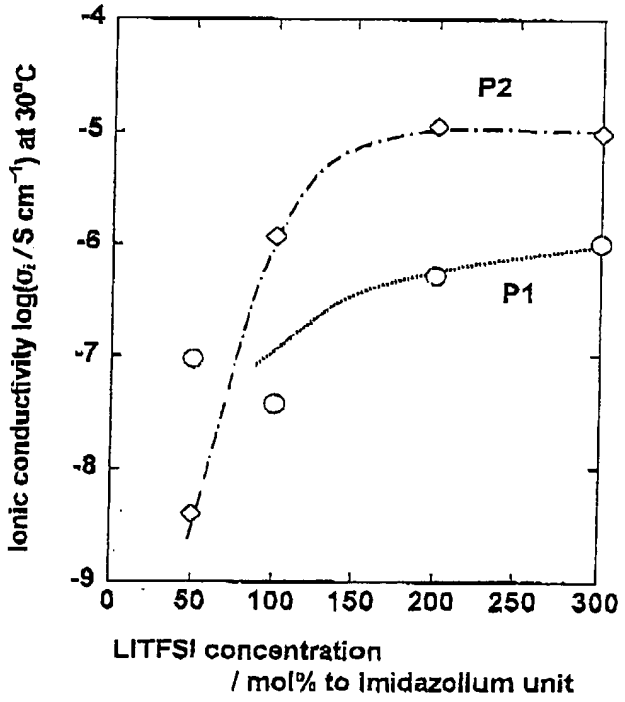

FIGURE 3. Effect of LiTFSI concentration on the ionic conductivity for P1 and P2.

one is the increase of free volume by the introduction of spacer group, and the other is the improvement of flexibility of ionic liquid moiety by the alkyl spacer. The introduction of spacer was effective to maintain the segmental motion high. The polymer systems having spacers onto cation site or both sites are now in progress.

The effect of LiTFSI concentration on the ionic conductivity of P1 or P2 was investigated. The ionic conductivity increased with increasing the amount of LiTFSI for both P1 and P2 as shown in Fig. 3. The ionic liquid copolymers containing excess LiTFSI (200 ~ 300 mol%) showed a constant ionic conductivity. The ionic conductivity of P2 is 10 ~ 20 times higher than that of P1. As mentioned above, this difference was based on the introduction of alkyl spacer. P2 maintains relatively high ionic conductivity at even high salt concentration. It is well known that the ionic conductivity of polyether systems was lowered by the addition of only small excess of salts. In poly(ethylene oxide) systems, the ionic conductivity decreased by the addition of small excess salts due to the elevation of Tg. We therefore attempted to discuss the different salt concentration dependence by means of Tg, however their Tg could not be determined with DSC measurement. This problem may be based on the distribution of molecular weight for these ionic liquid polymers. Continuous study has been carried out and results will be reported soon. It is possible to obtain more excellent ionic liquid polymers with higher ionic conductivity by the suitable molecular design of starting ionic liquid monomers.

CONCLUSION

We obtained novel ionic liquid copolymers prepared by the radical polymerization of 1-vinylimidazole neutralized with acids having vinyl group. Ionic liquid copolymer showed very low ionic conductivity of below 10^{-9} S cm^{-1} at 50 °C. When equimolar amount of LiTFSI was added, poly(vinylimidazolium-co-vinylsulfonate) showed the ionic conductivity of 7.2×10^{-7} S cm^{-1} at 50 °C. On the other hand, ionic liquid polymer having flexible spacer showed the ionic conductivity of 1.2×10^{-5} S cm^{-1} at 50 °C, which was about 20 times higher than that for polymer without spacer. It was revealed that flexible spacer is effective to improve the ionic conductivity of ionic liquid polymers after addition of salt.

ACKNOWLEDGMENTS

One of the authors (M. Y.) acknowledges the financial support of The Japan Society for the Promotion of Science (Research Fellowship for Young Scientist). The present study was supported by the Grant-in-Aid for Scientific Research from the Ministry of Education, Culture, Sports, Science and Technology, Japan (No. 11555250).

REFERENCES

1. Wilkes JS, Zaworotko MJ. Air and Water Stable 1-Ethyl-3-methylimidazolium Based Ionic Liquids. *J. Chem. Soc., Chem. Commun.* 1992; 965.
2. Fuller J, Carlin RT, De Long HC, Haworth D. Structure of 1-Ethyl-3-methylimidazolium Hexafluorophosphate: Model for Room Temperature Molten Salts. *J. Chem. Soc. Chem., Commun.* 1994;299.
3. Koch VR, Nanjundiah C, Appetecchi GB, Scrosati B. The Interfacial Stability of Li with Two New Solvent-Free Ionic Liquids: 1,2-Dimethyl-3-propylimidazolium Imide and Methide. *J. Electrochem. Soc.* 1995; 142: L116.
4. Bonhôte P, Dias A, Armand M, Papageorgiou N, Kalyanasundaram K, Grätzel M. Hydrophobic, Highly Conductive Ambient-Temperature Molten Salts. *Inorg. Chem.* 1996; 35: 1168.
5. Hagiwara R, Hirashige T, Tsuda T, Ito Y. Acidic 1-Ethyl-3-methylimidazolium Fluoride: A New Room Temperature Ionic Liquid. *J. Fluorine Chem.* 1999; 99: 1.
6. (a) MacFarlane DR, Meakin P, Sun J, Amini N, Forsyth M. Pyrrolidinium Imides: A New Family of Molten Salts and Conductive Plastic Crystal Phases. *J. Phys. Chem. B* 1999; 103: 4164. (b) MacFarlane DR, Huang J, Forsyth M. Lithium-Doped Plastic Crystal Electrolytes Exhibiting Fast Ion Conduction for Secondary Batteries. *Nature* 1999; 402: 792.
7. McEwen AB, Ngo HL, LeCompte K, Goldman JL. Electrochemical Properties of Imidazolium Salt Electrolytes for Electrochemical Capacitor Applications. *J. Electrochem. Soc.* 1999; 146: 1687.
8. Seddon KR. Ionic Liquids for Clean Technology. *J. Chem. Tech. Biotechnol.* 1997; 68: 351.
9. Welton T. Room-Temperature Ionic Liquids. Solvents for Synthesis and Catalysis. *Chem. Rev.* 1999; 99: 2071.
10. Itoh T, Akasaka E, Kudo K, Shirakami S. Lipase-Catalyzed Enantioselective Acylation in the Ionic Liquid Solvent System: Reaction of Enzyme Anchored to the Solvent. *Chem. Lett.* 2001; 262.
11. Huddleston JG, Willauer HD, Swatloski RP, Visser AE, Rogers RD. Room Temperature Ionic Liquids as Novel Media for 'Clean' Liquid-Liquid Extraction. *Chem. Commun.* 1998; 1765.
12. Wilkes JS, Levisky JA, Wilson RA, Hussey CL. Dialkylimidazolium Chloroaluminate Melts: A New Class of Room-Temperature Ionic Liquids for Electrochemistry, Spectroscopy, and Synthesis. *Inorg. Chem.* 1982; 21: 1263.
13. Hirao M, Sugimoto H, Ohno H. Preparation of Novel Room-Temperature Molten Salts by Neutralization of Amines. *J. Electrochem. Soc.* 2000; 147: 4168.
14. Yoshizawa M, Ogihara W, Ohno H. Design of New Ionic Liquid by Neutralization of Imidazole Derivatives with Imide-Type Acids. *Electrochem. Solid-State Lett.* 2001; 4: E25.
15. Fuller J, Breda AC, Carlin RT. Ionic Liquid-Polymer Gel Electrolytes form Hydrophilic and Hydrophobic Ionic Liquids. *J. Electroanal. Chem.* 1998; 459: 29.
16. Carlin RT, De Long HC, Fuller J, Trulore PC. Dual Intercalating Molten Electrolyte Batteries. *J. Electrochem. Soc.* 1994; 141: L73.
17. Noda A, Watanabe M. Highly Conductive Polymer Electrolytes Prepared by in situ Polymerization of Vinyl Monomers in Room Temperature Molten Salts. *Electrochim. Acta* 2000; 45: 1265.
18. Yoshizawa M, Hirao M, Ito-Akita K, Ohno H. Ion

Conduction in Zwitterionic-Type Molten Salts and Their Polymers. *J. Mater. Chem.* 2001; 11: 1057.
19. Ohno H. Molten Salt Type Polymer Electrolyte. *Electrochim. Acta* 2001; 46: 1407.
20. Hirao M, Ito K, Ohno H. Preparation and Polymerization of New Organic Molten Salts; N-alkylimidazolium salt derivatives. *Electrochim. Acta* 2000; 45: 1291.
21. Hirao M, Ito K, Ohno H. Polymerization of Molten Salt Monomers Having a Phenylimidazolium Group. *Polym. Adv. Technol.* 2000; 11: 534.
22. Yoshizawa M, Ohno H. Molecular Brush Having Molten Salt Domain for Fast Ion Conduction. *Chem. Lett.* 1999;889.
23. Yoshizawa M, Ohno H. Synthesis of Molten Salt-Type Polymer Brush and Effect of Brush Structure on the Ionic Conductivity. *Electrochim. Acta* 2001; 46: 1723.
24. Ohno H, Ito K. Room-Temperature Molten Salt Polymers as a Matrix for Fast Ion Conduction. *Chem. Lett.* 1998;751.
25. Yoshizawa M, Ogihara W, Ohno H. Preparation and Ionic conductivity of Molten Salt-Type Anionic Polymers. *Polymer Preprints, Japan* 2000; 49: 3213.
26. Takeoka S, Maeda Y, Kitahara Y, Tsuchida E. Ion Dissociation of Salts in Polyion Complexes and Adding Effect of Poly(oxyethylene). *Polymer Preprints, Japan* 1991; 40: 594.
27. Ohno H, Inoue Y, Wang P. Temperature-Controlled Ionic Conductivity Switching in Poly [oligo(oxyethylene) methacrylate]/Poly(ethylene oxide) layered Film. *Solid State Ionics* 1993; 62: 257.
28. Besner S, Vallee A, Bouchard G, Prud'homme J. Effect of Anion Polarization on Conductivity Behavior of Poly(ethylene oxide) Complexed with Alkali Salts. *Macromolecules* 1992; 25: 6480.

Liquid-Crystalline Assemblies Containing Ionic Liquids: An Approach to Anisotropic Ionic Materials

Masafumi Yoshio,† Tomohiro Mukai,† Kiyoshi Kanie, Masahiro Yoshizawa,† Hiroyuki Ohno,† and Takashi Kato*
Department of Chemistry and Biotechnology, School of Engineering, The University of Tokyo, Hongo, Bunkyo-ku, Tokyo 113-8656
†*Department of Biotechnology, Tokyo University of Agriculture and Technology, Koganei, Tokyo 184-8588*

(Received November 7, 2001; CL-011117)

Amphiphilic ionic liquid derivatives form self-organized lamellar liquid crystals with room temperature ionic liquids. The ionic conductivities along the smectic layers have been obtained for the samples aligned in the cells with electrodes. The highest value is 4.3×10^{-2} S cm^{-1} at 139 °C.

Liquid crystals combine order and mobility in molecular and supramolecular levels.[1,2] The control of the molecular alignment and the organized structures in the liquid-crystalline states can lead to the introduction of anisotropic functions for the organic optoelectronic and ion-conductive materials.[3] Recently, organic ionic liquids have attracted attention as electrolytes[4] and solvent media[5] for reactions and extractions because of their specific properties such as ion-conductive, non-volatile, and catalytic properties. Here, we intend to obtain anisotropic ion-active materials through self-organization of ionic materials. It has already been reported that ionic liquid derivatives having long alkyl chains alone show thermotropic smectic liquid crystallinity.[6] If these amphiphilic molecules can form the liquid-crystalline organized structures with ionic liquids, their ionic assemblies would be expected to function as anisotropic materials exhibiting high ionic conductivities. Their physical properties may also be easily tuned by the fraction of ionic liquids in the mixtures.

We report here a new class of self-organized systems, which is obtained by mixing of imidazolium ionic liquids and its amphiphilic derivatives having an octadecyl alkyl chain, as shown in Figure 1. The ionic conductivities of the self-organized materials have been examined.

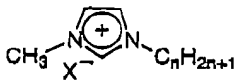

1a: X = BF_4, n = 18 2a: X = BF_4, n = 2
1b: X = PF_6, n = 18 2b: X = PF_6, n = 4

Figure 1. Structure of 1-methyl-3-alkylimidazolium salts.

Two room temperature ionic liquids **2a** and **2b**, which have hydrophilic and hydrophobic counter anions, respectively, have been selected to examine the ionic effects on the self-organization behavior for the amphiphilic molecules **1a** and **1b**. These compounds are prepared by N-alkylation of 1-methylimidazole with 1-bromoalkane, followed by the metathesis reaction using HBF_4 or HPF_6 aqueous solution.[6]

Figure 2 presents a phase diagram for the binary mixture of **1a** and **2a** as a function of the mole fraction of **2a**. Compound **1a** alone forms the thermotropic smectic A (S_A) and higher ordered smectic phases (S_X). For the mixtures of **1a** and **2a**, these smectic phases are observed up to the mole fraction of 0.6 for **2a** in the mixture. The isotropization temperatures are greatly decreased with the increase of the fraction of **2a**. The mixtures having more than the mole fraction of 0.7 of **2a** show no liquid crystallinity. For the mixture containing the smaller fraction of **1a** (0.5 wt%), the weak translucent gel is obtained below 50 °C.[7] Under polarizing microscopy, optically anisotropic fibrous aggregations are observed in the isotropic ionic liquid. For the mixtures consisting of **1b** and **2b**, no smectic liquid-crystalline phase is seen more than the mole fraction of 0.4 of **2b**.

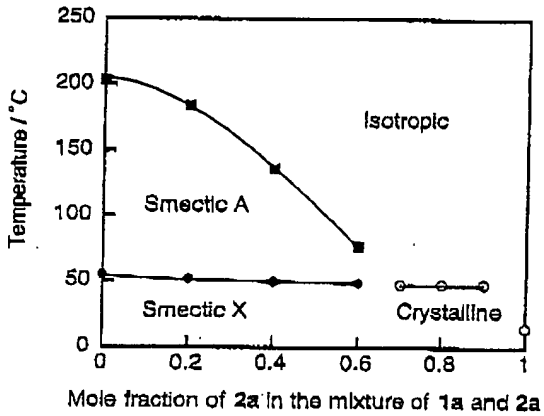

Figure 2. Phase transition behavior for the mixture of **1a** and **2a** on the heating runs.

Ion-conductive properties have been examined for compound **1a** alone and the self-organized mixture of **1a** and **2a**, which form the smectic liquid-crystalline phases.[8] A glass plate with comb-shaped gold electrodes (Au) and a pair of indium tin oxide (ITO) electrodes are employed for the anisotropic measurements of the ionic conductivity.[3f] For the samples forming the S_A phase, a homeotropic alignment is achieved on the glass surface with gold electrodes, which has been confirmed by polarizing microscopy, as schematically illustrated in Figure 3a. In this case, the ionic conductivities ($\sigma_{i//}$) along the direction parallel to the smectic-layer plane are measured for the aligned samples. In contrast, for the ITO electrodes, the ion-conductive values ($\sigma_{i\perp}$) along only direction perpendicular to the smectic-layer plane are not obtained because of polydomain formation, as illustrated in Figure 3b.

Figure 4 shows the ionic conductivities of compound **1a** and the mixture of **1a** and **2a** in the molar ratio of 3 : 2 (**1a**/**2a** = 3/2) as a function of temperature. The ionic conductivities for the samples homeotropically aligned in the S_A phases are higher than

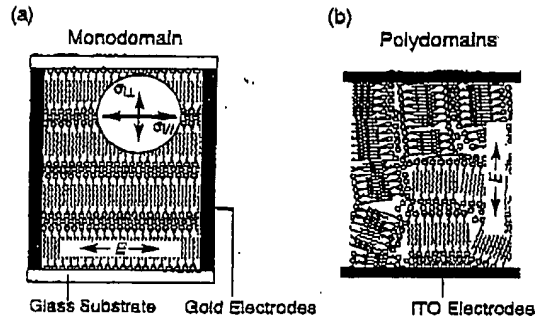

Figure 3. Schematic illustrations of the smectic liquid-crystalline ionic assemblies aligned with monodomain (a) and polydocains (b) on the glass surface with gold electrodes and on the ITO electrodes, respectively. *E*: Electric field..

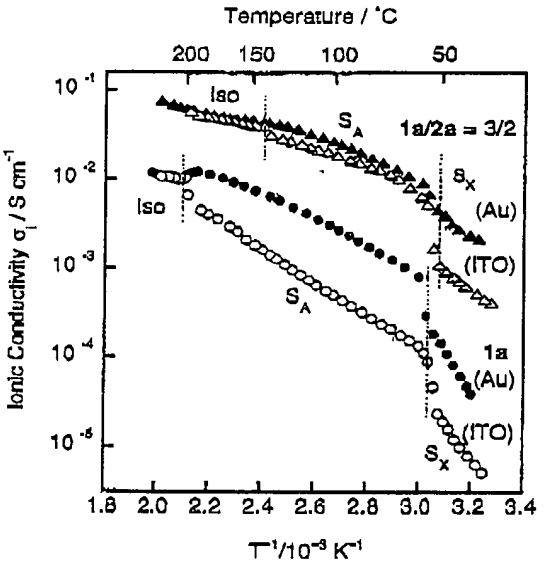

Figure 4. Ionic conductivities for the smectic liquid-crystalline samples of **1a** alone and **1a/2a**, which are aligned with monodomain (●, ▲) and polydomains (○, △) on the glass surface with gold electrodes and on the ITO electrodes, respectively.

those for the samples with polydomains. When the liquid-crystalline order disappears at the isotropization temperatures on heating, the ionic conductivities for the samples filled in the both cells with Au and ITO electrodes show no difference due to the disorder of the mixture. The formation of anisotropic long-range conductive pathways in the homeotropically aligned S_A phases should contribute to high ionic conductivities. The incorporation of mobile simpler ionic liquid into these pathways enhances the ionic conductions in the layered structures. The $\sigma_{i//}$ values for the homeotropically aligned mixture forming the S_A phase become about 10 times higher than those for **1a** alone.

It was reported that the ionic conductivities of isotropic ionic liquids alone gradually increase with the increase in temperature.[4b] In contrast, for the mesomorphic materials in the present study, the discontinuous changes of ionic conductivities are observed at the phase transitions. For example, the ionic conductivities ($\sigma_{i//}$) for the aligned sample of **1a** increase at 55 °C and decrease at 203 °C on heating. These temperatures correspond to the S_X-S_A and S_A-Isotropic (Iso) transitions, respectively. The isotropic ionic conductivity of the single component of **2a** at 30 °C is 2×10^{-2} S cm^{-1},[9] while the anisotropic ionic conductivity ($\sigma_{i//}$) of **1a/2a** in the molar ratio of 3 : 2 is 2×10^{-3} S cm^{-1} at the same temperature. It is noteworthy that the liquid-crystalline assemblies keep relatively high ionic conductivities even though insulating aliphatic layers are incorporated.

Amphiphilic ionic molecules presented here form the self-organized lamellar liquid crystals with room temperature ionic liquids. These liquid crystals are novel functional materials, which show anisotropic ion-active properties. The ionic conductivities of the organized materials are tunable by the change of the fraction of ionic liquids.

References and Notes

1 "Handbook of Liquid Crystals," ed. by D. Demus, J. W. Goodby, G. W. Gray, H.-W. Spiess, and V. Vill, Wiley-VCH, Weinheim (1998).
2 a) T. Kato, *Struct. Bonding*, **96**, 95 (2000). b) C. K. Ober and G. Wegner, *Adv. Mater.*, **9**, 17 (1997).
3 For example: a) J. Ruokolainen, R. Mäkinen, M. Torkkeli, T. Mäkelä, R. Serimaa, G. ten Brinke, and O. Ikkala, *Science*, **280**, 557 (1998). b) F. B. Dias, S. V. Batty, G. Ungar, J. P. Voss, and P. V. Wright, *J. Chem. Soc., Faraday Trans.*, **92**, 2599 (1996). c) M. Funahashi and J. Hanna, *Phys. Rev. Lett.*, **78**, 2184 (1997). d) K. Akagi, H. Goto, H. Shirakawa, *Synth. Met.*, **84**, 313 (1997). e) T. Kato, Y. Kubota, and T. Uryu, *Polym. Bull.*, **38**, 551 (1997). f) T. Ohtake, M. Ogasawara, K. Ito-Akita, N. Nishina, S. Ujiie, H. Ohno, and T. Kato, *Chem. Mater.*, **12**, 782 (2000).
4 a) P. Bonhôte, A.-P. Dias, N. Papageorgiou, K. Kalyanasundaram, and M. Grätzel, *Inorg. Chem.*, **35**, 1168 (1996). b) A. B. McEwen, H. L. Ngo, K. LeCompte, and J. L. Goldman, *J. Electrochem. Soc.*, **146**, 1687 (1999).
5 a) T. Welton, *Chem. Rev.*, **99**, 2071 (1999). b) P. Wasserscheid and W. Keim, *Angew. Chem., Int. Ed.*, **39**, 3772 (2000).
6 a) C. M. Gordon, J. D. Holbrey, A. R. Kennedy, and K. R. Seddon, *J. Mater. Chem.*, **8**, 2627 (1998). b) J. D. Holbrey and K. R. Seddon, *J. Chem. Soc., Dalton Trans.*, **1999**, 2133.
7 The detail in this gel behavior will be reported elsewhere.
8 Dynamic ionic conductivities of the liquid-crystalline samples were measured with the complex-impedance method using an impedance analyzer (Schlumberger, Solarton 1260 and a custom set-up temperature controller).
9 A. Noda and M. Watanabe, *Electrochim. Acta*, **45**, 1265 (2000).

Chapter 23

Characterization of Hydrophilic and Hydrophobic Ionic Liquids: Alternatives to Volatile Organic Compounds for Liquid–Liquid Separations

Ann E. Visser, W. Matthew Reichert, Richard P. Swatloski, Heather D. Willauer, Jonathan G. Huddleston, and Robin D. Rogers*

Department of Chemistry and Center for Green Manufacturing, The University of Alabama, Tuscaloosa, AL 35487

Herein we describe the physical and chemical properties for several Ionic Liquids (ILs) comprised of the 1-alkyl-3-methylimidazolium cation with the Cl^-, Br^-, I^-, BF_4^-, or PF_6^- anions. Liquid-liquid separations with the PF_6^- ILs are highlighted to illustrate their use in "Green Chemistry," as alternatives to traditional organic solvents in separations. The partitioning of organic molecules, combined with IL characterization, has facilitated successful metal ion extraction with both anionic and molecular extractants. This report discusses our current results in the characterization of ILs, their use in liquid-liquid extraction, new concepts for metal ion separations, and solid-state analyses.

Introduction

The curiosity surrounding Ionic Liquids (ILs) has focused on their unique properties, particularly as alternatives to traditional organic solvents in synthesis (*1*) and in liquid-liquid separations from aqueous solutions (*2-6*). Separation

processes employing liquid-liquid extractions are a common industrial unit operation, the characteristics of the extracting phase can be fine tuned by selection from the many organic solvents available (*7*). However, most common solvents are volatile organic compounds (VOCs), and their associated chemical behavior (in addition to their potential toxicity) classifies many of them as hazardous substances.

Green Chemistry

Early social perceptions of chemistry and the chemical industry centered on innovations in medicine, technology, and the overall improvement in the quality of life. More recently, with the rapidly expanding chemical industry, those perceptions have changed and many perceive the industry as a major contributor towards air, land, and water pollution. Each year, the U.S. produces millions of tons of pollution and, at the same time, spends tens of billions of dollars controlling this pollution in the production and cleanup cycle. Therein is the indication that redesigning of chemical production processes may be more effective through targeting source reduction instead of "end of the pipe" waste management or pollution control (*8*). Ideally, pollution would be controlled or minimized at the source, recycling would be done if possible, and any unavoidable waste production would be handled in an appropriate manner.

The chemical industry realizes that their sustained future growth, revenue, and scientific development may depend on considering how their production practices and technologies impact the health and safety of their employees and the environment. Major laws, such as the Clean Air Act and Pollution Prevention Act, have been the impetus for many of these changes (*8*).

Subsequently, the idea of "Green Chemistry" was established to promote the research, development, and implementation of innovative chemical technologies to achieve pollution prevention in a technologically and economically sound manner (*8*). All this would be achieved, from the green chemistry standpoint, through technologies that reduce the consumption or production of hazardous chemicals during the manufacturing or processing of chemical products. A decrease in the generation of hazardous chemicals, along with a diminished potential for health and environmental problems, would be the direct result of a new paradigm for chemical manufacturing or processing.

New Solvent Technologies

Many chemicals that are routinely used are a necessary part of the manufacturing process and yet dangerous to health and the environment. The penchant for traditional solvent extraction systems has come to a crossroads as

the emphasis for sustainable technology and green chemistry considers the overall environmental impact of both the process and waste streams generated as a result.

We have been investigating ILs and polymer-based Aqueous Biphasic Systems (ABS) as alternatives to traditional organic solvents in liquid-liquid separations. Although both areas have their own specialized literature, several reports highlight separations based on ILs (*3,10-12*) or ABS (*13-15*) where the merits of both systems show their potential for implementation into industrial separations systems. Most notable from a "Green" perspective is the fact that both ABS and ILs can be used in place of VOCs in liquid-liquid separations. Other work on novel solvent media has shown how supercritical water (*16,17*), supercritical CO_2 (*9*), solventless phases (*18*), and fluorous phases (*19*) can be used in an effort to broaden the scope of possibilities available for more environmentally responsible processes.

Room Temperature Ionic Liquids (RTILs)

RTILs (or, more generally, ILs), as discussed in this book, are a class of novel compounds composed entirely of ions that, together, melt at or below ambient temperatures (or below 150 °C for ILs) and may be thought to resemble molten ionic melts such as NaCl at 800 °C. While both ILs and molten salts are composed of ions, the presence of organic cations in ILs interrupts the crystal packing and lowers the melting point. Depending on the composition, the resulting IL can be hydrophobic or hydrophilic. An inherent property of many ILs is their miniscule volatility and easily manipulated properties, characteristics of a unique class of solvents. Literature reports are awash with cations for use in these systems, including ammonium (*20-22*), pyridinium (*23,24*), pyrrolidinium (*25*), isoquinolinium (*26*), and imidazolium (*2,27*), each with the possibility for attaching various alkyl groups to the ring or quaternary onium cation. Depending on the type of cation investigated and the length of the alkyl chain, the resulting salts may have a melting point above room temperature and several crystal structures have been reported (*28*).

In our research, we have focused on RTILs incorporating the 1-alkyl-3-methylimidazolium ($[C_nmim]^+$) cation, as shown in Figure 1 (*2-4*). The alkyl group is usually an *n*-alkane and increasing the length of the alkane chain affects the resulting properties (e.g., viscosity, hydrophobicity, and melting point (*2,27*)). For example, $[C_8mim][PF_6]$ is a liquid at room temperature with a glass transition temperature at –75 °C (*2*) and $[C_{10}mim][PF_6]$ melts at 38 °C (*3*). RTILs composed of several different cations or anions (i.e., multi-component mixtures) can be envisaged to further expand the family of ionic liquids.

IL cations and anions can be used to control the water miscibility of the resulting ILs and the choice of anion has been used to the greatest effect on

controlling hydrophobicity. 1-alkyl-3-methylimidazolium salts of PF_6^- are water immiscible; BF_4^- salts are water miscible depending on alkyl chain length, and tetrahaloaluminate salts are moisture sensitive. Fluorinated anions such as $N(SO_2CF_3)_2^-$ impart even greater hydrophobicity despite increased expense (*27*).

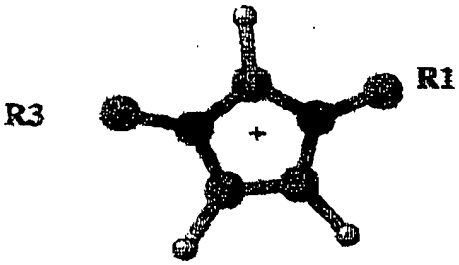

R3 = CH_3; R1 = *n*-alkane

Figure 1. Generic cations for 1-alkyl-3-methylimidazolium RTILs.

The ionic liquids we have used in our liquid-liquid studies are all liquids below 40 °C, although 150 °C is the adopted upper temperature limit for 'ionic liquid' classification. RTIL is an arbitrary subdivision of ILs that are liquid at room temperature and, thus, facilitate their use at ambient temperatures. Here, we will provide an overview of organic partitioning and metal ion extraction in RTIL-aqueous systems with particular focus on the effects of anion selectivity, increasing alkyl chain length, and cation substitution.

Experimental

The experimental details for the data and procedures reported here are provided in references to physical properties (*2*), organic solute partitioning (*29*), and metal ion extraction (*4-6*). Distribution ratios as reported here are defined as the ratio of the solute concentration in the RTIL lower phase divided by the solute concentration in the aqueous upper phase.

Thymol blue (*3*) partitioning was measured via UV-Vis spectroscopy while the remaining organic solute and metal ion studies reported here utilized radio-labeled chemicals. The methods for chemical and physical characterization of the ILs are described elsewhere (*2*).

Results

Partitioning of Organic Solutes

Our initial results (*29*) for aromatic solute partitioning between water and $[C_4mim][PF_6]$ indicated that neutral, hydrophobic, aromatic solutes have an affinity for the ionic liquid phase, as shown in Figure 2. For the simple benzene derivatives investigated, partitioning to the RTIL phase generally increased in accordance with the solutes' 1-octanol-water log P values, a common measure of solute hydrophobicity. This demonstrated that partitioning could be achieved and, in many cases, partitioning can be predicted (and/or modeled) using traditional solvent extraction parameters. In this manner, ILs behaved as conventional solvents, displaying a noticeable affinity for aromatic solutes and low aliphatic solubility. Once in the RTIL phase, volatile organic solutes can be removed by distillation or pervaporation, as the RTILs themselves may have negligible vapor pressure. Many non-volatiles can be removed through contact with supercritical CO_2 (*9*). The solubility of $[C_nmim][PF_6]$ in various ethanol-water solutions (*30*) suggests complex solution behavior with increasing mole fractions of traditional solvents.

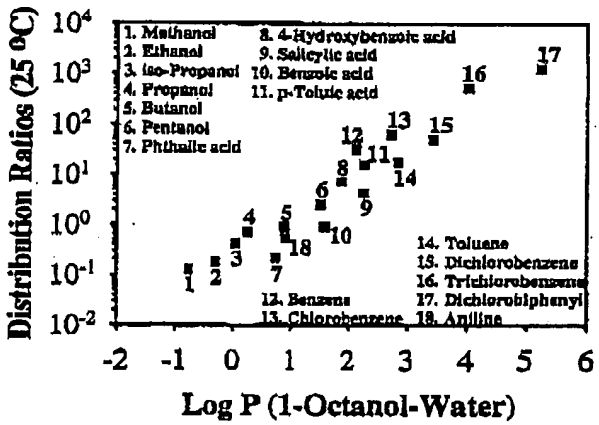

Figure 2. Distribution ratios of organic solutes for the $[C_4mim][PF_6]$-water biphasic system; data from ref. (29).

With charged or ionizable solutes, a change in the aqueous phase pH resulted in certain ionizable solutes exhibiting pH-dependent partitioning such that their affinity for the RTILs decreased upon ionization (*29*). As shown in Figure 3, solute ionization affects the partitioning of aniline and benzoic acid and may be sufficient to cause several orders of magnitude difference in the

partitioning. Thus, for ionizable solutes, a change in aqueous phase pH could be used for solute recovery from the RTIL phase.

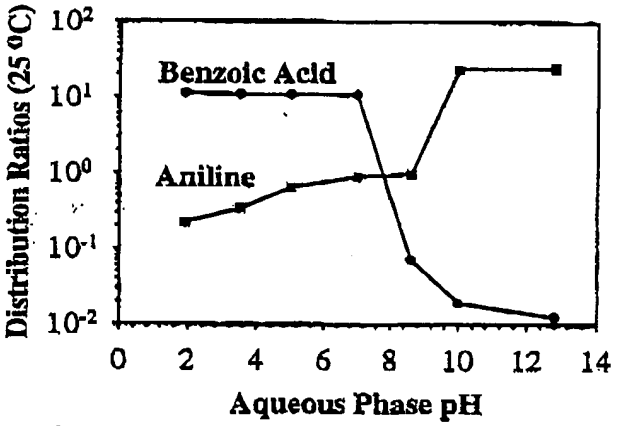

Figure 3. Distribution ratios for aniline (pK_b = 9.42) and benzoic acid (pK_a = 4.19) in [C_4mim][PF_6]-aqueous systems as a function of aqueous phase pH.

Other solutes may have substituent groups that hinder their solubility and partitioning in RTIL-water systems. We have studied the partitioning of unsubstituted, *t*-butyl-, and sulfonated-calixarenes in a series of [$C_n$mim][PF_6]-water systems as a function of aqueous phase pH (*31*). The hydrophobic nature of the RTILs offers an environment suitable for solubilizing the unsubstituted calix-4 and calix-6-arenes, where distribution ratios for both molecules are above 100 and are relatively unaffected by aqueous phase pH. However, the *t*-butyl-calixarenes were not soluble in these RTILs. Adding sulfonate groups to the calixarenes diminished their affinity for the RTIL phase and distribution ratios indicate those molecules prefer the aqueous phase.

We further investigated the pH dependent partitioning of the cationic dye, thymol blue, in these systems (*3*). As depicted in Figure 4, thymol blue preferred the RTIL phase in both the zwitterionic and monoanionic form and partitioned to the aqueous phase under basic conditions. Of the RTILs investigated in liquid-liquid partitioning experiments, thymol blue distribution ratios increased with RTIL hydrophobicity (or lipophilicity) and were highest in [C_8mim][PF_6]. Solid-liquid separations were performed with [C_{10}mim][PF_6] to illustrate how successive heating, mixing, and cooling, combined with appropriate pH changes, could remove thymol blue from an aqueous phase with no retention of the dye upon recrystallization of [C_{10}mim][PF_6] (*3*).

The behavior of organic solutes in RTIL systems illustrates both the unique and unexpected characteristics of RTIL-based separations. With respect to organic solutes, traditional descriptors provide a good indication of solute

affinity for the RTIL phase. For ionizable molecules, ionization has an apparent effect on phase affinity and may provide a facilitated means for stripping. When selecting or modifying a RTIL, the resulting hydrophobicity has a significant impact on partitioning results.

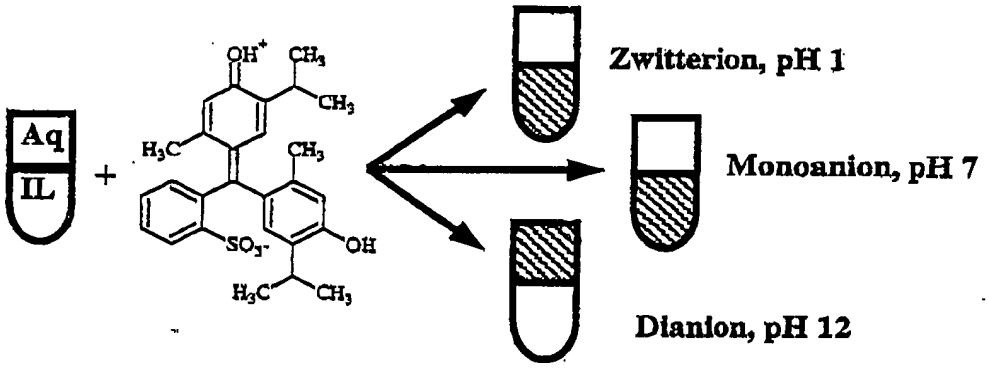

Figure 4. Behavior of thymol blue in [$C_n$mim][PF_6]-aqueous biphasic systems as a function of aqueous phase pH (3).

Metal Ion Extraction

In liquid-liquid separation systems, the hydrated nature of most metal ions lowers their affinity for the extracting phase. This is the case in RTIL systems where hydrated metal ions do not partition to ILs from water (*5,32*). Therefore, it is necessary to change the hydration environment of the metal ion by either using organic ligands (*33-35*) which provide a more hydrophobic region around the metal or form neutral compounds, or with inorganic anions (*36*) that form softer more extractable anionic complexes with the metal. Ideally, in a biphasic system, the extractant would remain in the hydrophobic phase to ensure the complete removal of the metal ions from the aqueous phase. Thus, the challenges in adapting new classes of solvents to traditional separations include finding extractants which quantitatively partition to the solvent phase and can still readily complex target metal ions; or finding conditions under which specific metal ion species can be selectively extracted from aqueous streams containing inorganic complexing ions.

Organic Extractants

Our initial studies used 1-(2-pyridylazo)-napthol (PAN) and 1-(2-thiazolyl)-2-napthol (TAN) as extractants for metal ions in light of their success in

polymer-based ABS (*37*) and traditional solvent extraction systems (*38*). These are conventional metal extractants widely used in solvent extraction applications. When the aqueous phase is basic, both molecules are ionized, yet they quantitatively partition to $[C_6mim][PF_6]$ over the pH range 1-13. As other reports indicate (*39*), the ionization of the molecules plays an important role in the metal ion extraction, as shown in Figure 5. The distribution ratios for Fe^{3+}, Co^{2+}, and Cd^{2+} show that metal ions could be extracted from the aqueous phase at basic pH and stripped from the RTIL under acidic conditions.

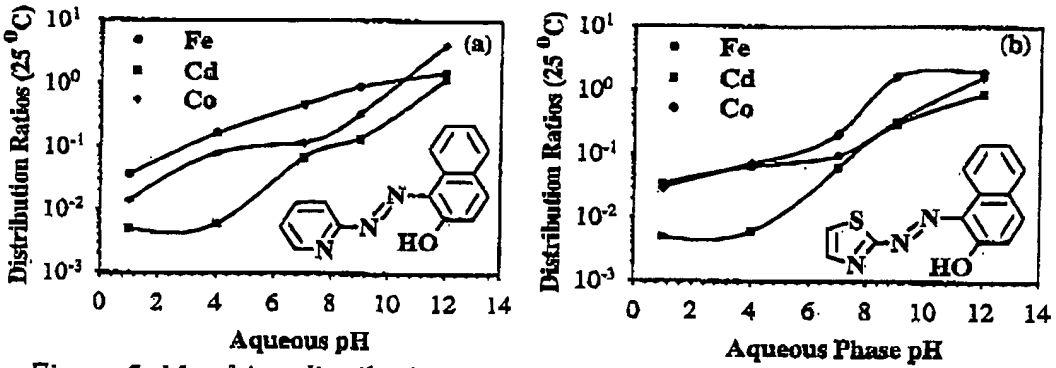

Figure 5. Metal ion distribution ratios with 0.1 mM PAN (a) or TAN (b) in $[C_6mim][PF_6]$-aqueous systems as a function of aqueous phase pH (37).

Macrocyclic ligands such as crown ethers have been widely used for metal ion extraction (*35,40*). The structure and cavity size of the crown ether is the basis for metal ion selectivity and by attaching alkyl or aromatic ligands to the crown, the hydrophobicity of the ligand can be adjusted. Others have used dicyclohexano-18-crown-6 as an extractant for Sr^{2+} in $[C_nmim][N(SO_2CF_3)_2]$ RTIL liquid-liquid systems with impressive results (*11*). However, the conditions for optimal extraction in the RTIL system (i.e., low HNO_3 concentrations) were unexpected and contrary to what is typically employed in solvent extraction (*40*). We have used 18-crown-6, dicyclohexano-18-crown-6, and 4,4'-(5')-di-(*t*-butylcyclohexano)-18-crown-6 as extractants for Sr^{2+}, Cs^+, and Na^+ in $[C_nmim][PF_6]$-aqueous systems (*4*). Our results for the partitioning from HNO_3 are contrary to traditional solvent extraction behavior in that while the most hydrophobic extracting phase usually produces the highest distribution ratios, as expected, distribution ratios decrease with increasing acid concentrations.

It was noted, however, that in the presence of increasing HNO_3 (i.e., 1 - 8 M), the degradation of PF_6^- to PO_4^{3-} significantly increased the hydrophilicity of the RTIL phase and produced a monophasic system. Using $Al(NO_3)_3$ as the

source of the nitrate anion leads to an increase in distribution ratios (Figure 6) and precluded the degradation of PF_6^- observed at high concentrations of HNO_3. Our results indicate that metal ion partitioning is very complex in RTIL-based liquid-liquid systems and other factors such as aqueous phase composition and water content of the RTILs have dramatic effects on both the metal ion extraction and the stability of the RTILs.

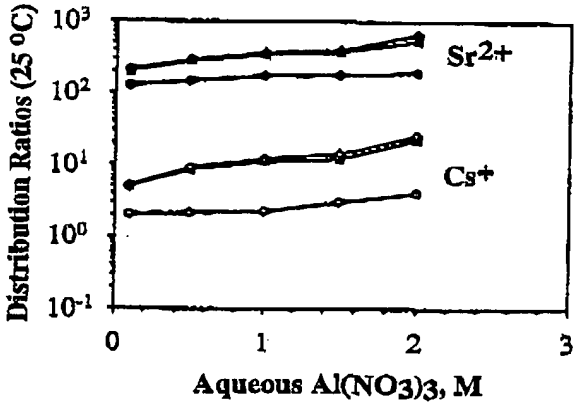

Figure 6. Sr^{2+} and Cs^+ distribution ratios with 0.1 M di-tertbutyl-dicyclohexano-18-crown-6 in $[C_nmim][PF_6]$-aqueous systems ($[C_4mim]^+$ (●), $[C_6mim]^+$ (■), $[C_8mim]^+$ (◆)) with increasing aqueous phase concentrations of $Al(NO_3)_3$ (4).

Anionic Extractants

The distribution ratios of certain metal ions may be enhanced in the presence of complexing anions such as halides or pseudohalides. Metal ions such as Hg^{2+} have large formation constants with halides (*41*) and their effect has been observed on the partitioning of Hg^{2+} in other systems (*42*). We have used halides, cyanate, cyanide, and thiocyanate as anionic extractants for metal ion partitioning in $[C_4mim][PF_6]$-aqueous systems (*5*) and the results are shown in Figure 7. For the halides, the formation constants for the series of Hg-I complexes are the highest and decrease to those for Hg-F (*41*). That, in combination with the relative hydrophobicity of the complexes, explains why the iodide complexes produce the highest distribution ratios. The results with the pseudohalides, however, suggest a more complex partitioning mechanism since the Hg-CN complexes have the highest formation constants (*41*), yet display the lowest distribution ratios, similar to data found in other separations systems (*42*).

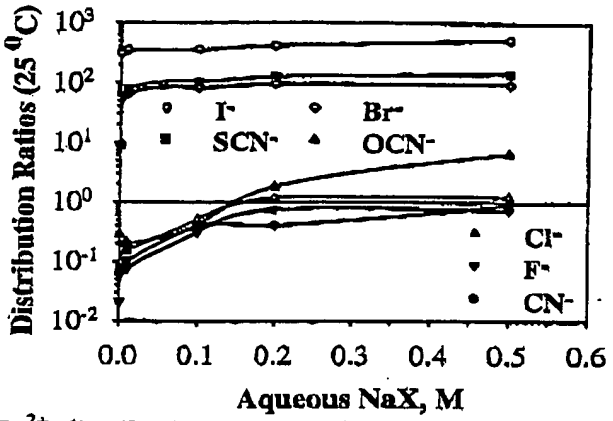

Figure 7. Hg^{2+} distribution ratios with increasing aqueous halide or pseudohalide concentrations in $[C_4mim][PF_6]$-aqueous systems (5).

Task Specific Ionic Liquids

Through a collaboration with the Davis Group at the University of South Alabama, Task Specific Ionic Liquids (TSILs) have been utilized for metal ion separations. Here, known metal ion ligating groups are incorporated into the cationic moiety of the IL by tethering to the imidazolium cation (Figure 8).

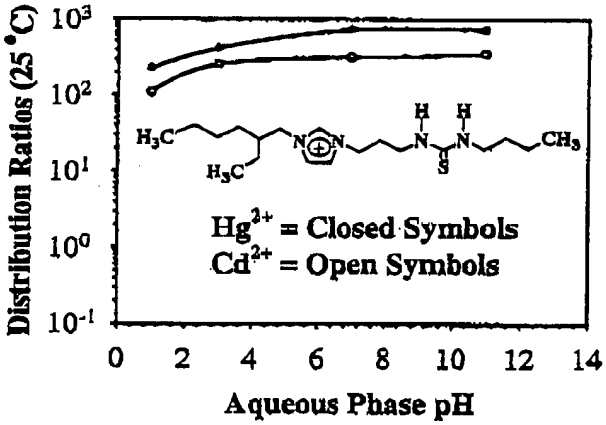

Figure 8. Hg^{2+} and Cd^{2+} distribution ratios from water to RTIL phases comprised of 1:1 combinations of $[C_4mim][PF_6]$ and a TSIL (6).

We have used thioether, urea, and thiourea derivatized imidazolium cations in conjunction with PF_6^- for the extraction of Hg^{2+} and Cd^{2+} (6). As shown in Figure 8, distribution ratios are typically higher for Hg^{2+} and a change in the

aqueous phase pH has a slight effect on the partitioning. (Thus, alternate routes may be necessary for significant metal ion stripping.) Depending on the properties of a specific TSIL, it can be used as the extracting phase or, if the TSIL melts above room temperature, in a combination with $[C_4mim][PF_6]$ as the extracting phase (*6*).

Physical Properties

Utilization of RTILs in solvent extraction technologies requires detailed knowledge of the solvents' physical properties (e.g., hydrophobicity, viscosity, density, surface tension, etc.). Both hydrophobic and hydrophilic RTILs have their niche, although each type may be uniquely suited for certain applications including synthesis, catalysis (*43*), and separations. We have utilized RTILs incorporating either the PF_6^-, $N(SO_2CF_3)_2^-$, and $N(SO_2CF_2CF_3)_2^-$ ([BETI]) anions to produce hydrophobic RTILs suitable for use in place of organic solvents for separations (2). (It should be noted that certain combinations (though not all) of imidazolium and pyridinium cations and $N(SO_2CF_3)_2^-$, $N(SO_2CF_2CF_3)_2^-$, and other hydrophobic anions are covered by U. S. Patent 5,827,602 (*44*).)

Solvent choice can have a substantial effect on the reaction conditions since parameters such as solvent polarity, density, and viscosity impact not only the solute environment, but also the associated engineering considerations. With traditional organic solvents, associated properties include high solute capacity, solute compatibility, and fine-tunability, although it is their volatile nature that has raised the most concern and initiated the search for solvent alternatives.

Table I is a summary of the properties for water-equilibrated [1-alkyl-3-methylimidazolium][PF_6] RTILs, as employed in many of our liquid-liquid experiments. Our previous results (2) indicate water content has a profound effect on certain properties and, in liquid-liquid separation systems analyses after equilibration with water provide the most accurate data needed for engineering RTIL processes under those conditions. The data in Table I is representative for hydrophobic RTILs in comparison to the corresponding hydrophilic RTILs listed in Tables II and III.

Despite the fact that RTILs incorporating the PF_6^- anion sustain biphasic systems, after contact with water they contain a significant, albeit non-stoichiometric, amount of water. We have shown that, for example, the water content for $[C_4mim][PF_6]$ decreases to 590 ppm after a period of drying (2), although the resulting $[C_4mim][PF_6]$ is hygroscopic and rapidly adsorbs atmospheric water to return to the saturation point. The RTILs can be successively dried by heating under vacuum. Previous partitioning results show that an increase in the alkyl chain length produces higher distribution ratios (*3*) for hydrophobic solutes, confirming the increase in RTIL hydrophobicity and lipophilicity.

Table I. Properties of Water-Equilibrated [$C_n$mim][PF_6] RTILs (2)

Parameter	*[C_4mim] [PF_6]*	*[C_6mim] [PF_6]*	*[C_8mim] [PF_6]*
Water content (ppm)	11700	8837	6666
Viscosity (cP, 25 °C)	397	452	506
Density (g/mL)	1.35	1.24	1.16
Melting point (°C)	4	na[a]	na
Glass transition temperature (°C)	-86	-75	-75
Thermal decomposition (°C, onset)	360	390	374
Surface tension (dyn/cm)	49.8	36.8	34.2

[a] na = transition not observed.

$[C_n mim]^+$ ($n \leq 4$) combined with halides or BF_4^- (*45*) produce hydrophilic ILs that have subtly different properties, as shown in Tables II and III, respectively. In reality, a switch from hydrophilic to hydrophobic RTILs is a continuum that can be modified by changes in anion type and cation substitution. Other cation types, for example PR_4^+, offer alternatives, especially lipophilic, hydrophobic systems which have densities less than 1 which could be used in conventional solvent extraction flotation systems. In Tables II and III, it is important to consider that these RTILs were characterized after being 'dried' for 4 – 5 h at 70 °C under reduced pressure.

Table II. Properties of Dried[a] Hydrophilic [$C_n$mim][Cl] ILs (2)

Parameter	*[C_4mim] [Cl]*	*[C_6mim] [Cl]*	*[C_8mim] [Cl]*
Water content (ppm)	2200	1130	890
Viscosity (cP, 25 °C)		716	337
Density (g/mL)	1.08	1.03	1.00
Melting point (°C)	41	na	na
Glass transition temperature (°C)	na	-75	-87
Thermal decomposition (°C, onset)	254	253	243
Surface tension (dyn/cm)		42.5	33.8

[a] dried = heating to 70 °C for 4 – 5 h while stirring, under reduced pressure.

The properties in Tables I-III confirm that compromises may be necessary when selecting an optimal IL for a particular application. Although many cation and anion combinations are available, it is evident that concessions must be made between hydrophobicity, viscosity, expense, etc. The majority of these anions are non-coordinating, although the relatively high melting point for

$[C_4mim][Cl]$ suggests that the cation-anion interactions facilitate hydrogen bonding.

Table III. Properties of Dried[a] Hydrophilic $[C_4mim][BF_4]$ and $[C_4mim][I]$ ILs (2)

Parameter	*$[C_4mim][BF_4]$*	*$[C_4mim][I]$*
Water content (ppm)	4530	1870
Viscosity (cP, 25 °C)	219	1110
Density (g/mL)	1.12	1.44
Glass transition temperature (°C)	-97	na
Thermal decomposition (°C, onset)	403	265
Surface tension (dyn/cm)	46.6	54.7

[a] dried = heating to 70 °C for 4 – 5 h while stirring, under reduced pressure.

In general, rheological properties of the RTILs vary with water content. For example, increasing the water content usually reduces viscosity. For $[C_8mim]^+$, the longer alkyl chain produces a more viscous RTIL while $[C_4mim]^+$, by contrast, has the lowest viscosity. Small amounts of chloride remaining from the synthesis may also act to increase the viscosity (*46*).

Density in the ILs described here decreases as the size of the cation increases since the mass of CH_2 is less than that for an imidazolium ring. In addition, as the cation size increases, surface tension decreases which can be attributed to greater charge dispersion over the cation and the associated effect on the cation-anion interactions. Ordinarily, these properties would be expected to change in a similar manner; increasing the cation size would increase both the viscosity and surface tension. Thus, viscosity and surface tension, both parameters that are highly dependent on intermolecular interactions, appear to be determined by different interactions in the ILs.

Thermal properties such as glass transition temperatures and the onset of thermal decomposition are essentially independent of the composition for these $[C_nmim][PF_6]$ RTILs. In general, a class of cations will show glass transition temperatures around a similar temperature range (*25,47,48*). Here, the glass transition temperature is around –80 °C and is close to that for other imidazolium-based RTILs (*45*). A glass transition requires cation and anion reorganization to produce a more ordered material. The addition of CH_2 groups to the alkyl chain may require a minimal amount of additional thermal energy to produce the transition, hence the similarity in these results. Melting points, on the other hand, are not observed for $[C_6mim][PF_6]$ and $[C_8mim][PF_6]$, further supporting the observed tendency for RTILs to supercool.

When designing a RTIL, fine-tuning the properties can be achieved by changing the cation substituent groups, anion identity, or by mixing two types of RTILs with differing, but defined characteristics. For example, the combination of a TSIL with [C_4mim][PF_6] can be used for Hg^{2+} and Cd^{2+} extraction (*6*). Incorporating anions to produce hydrophilic RTILs illustrates a wider range of properties, as shown in Table II. The effect of anion identity and, as a result, water content on the properties is obvious by comparison of Tables I-III.

Recently, we have prepared a series of RTILs containing 1-alkyl-isoquinolinium cations, combined with the bis(perfluoroethylsulfonyl)imide ($N(SO_2CF_2CF_3)_2^-$, [BETI]) anion, to produce a new class of ILs. We have also pursued their characterization and use in separations (*26*). The physical properties for [$C_n$isoq][BETI] are summarized in Table IV.

Table IV. Properties of Water-Equilibrated [$C_n$isoq][BETI] ILs (*26*)

n	*Water Content (ppm)*	*Melting Point (°C)*	*Glass Transition (°C)*
4	17700	-62.0	-85.2
6	16200	-77.3	-84.0
8	14900	-68.1	-79.4
10	6900	-59.3	-77.8
12	6600	-51.0	-75.4
14	6100	-49.7	-66.7
16	4700	-48.6	-61.8
18	4100	-47.2	-59.3

As the alkyl chain length ranges from butyl to octadecyl within this series, the hydrophobicity shows an order of magnitude increase. [C_8isoq][BETI] and [C_{14}isoq][BETI] were used in liquid-liquid partitioning experiments for a series of organic molecules (Figure 9) (*26*). Increasing the solute hydrophobicity (as denoted by the 1-octanol-water log P value produces increasing distribution ratios that are slightly higher in [C_{14}isoq][BETI] compared to [C_8isoq][BETI], congruent with the water content. In particular, the distribution ratios for 1,2,4-trichlorobenzene in [C_{14}isoq][BETI] is 1280 (6100 ppm water) compared to 1130 in [C_8isoq][BETI] (14900 ppm water). Using [C_4mim][PF_6] (11700 ppm water) as the extracting phase, the distribution ratio is 524 (*29*).

Here, the composition of the IL makes significant contributions towards the partitioning results. Upon equilibration with water, [C_{14}isoq][BETI] contains more water than water-equilibrated [C_4mim][PF_6] (*2*), although the distribution ratios for 1,2,4-trichlorobenzene are much higher than in [C_4mim][PF_6]. It is not yet clear whether the extended aromatic region in $[C_{14}isoq]^+$ promotes interactions with aromatic solutes or if the observed trends are due to the extended hydrophobic environment offered by the longer alkyl chains.

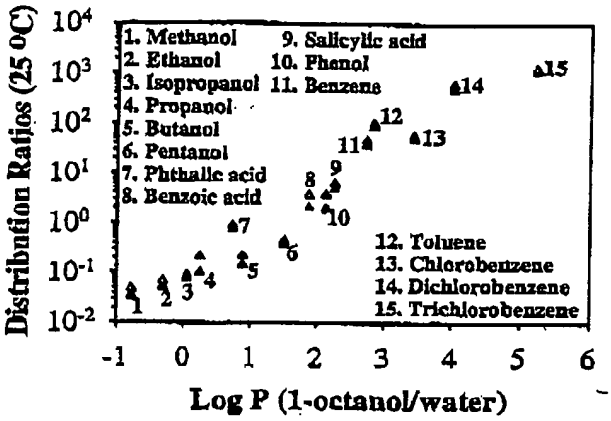

Figure 9. Distribution ratios for organic solutes from water to [C_8isoq][BETI] (▲) or [C_{14}isoq][BETI] (△) systems as a function of the solutes' 1-octanol-water log P values.

Crystal Structures

Since the scientific community has suggested an arbitrary 150 °C as an upper limit on "Ionic Liquid" melting points, there are many cation and anion combinations that produce crystalline materials that can be investigated to further understand the interactions in these systems. Parameters such as cation substitution and anion identity have been selected to investigate their contribution towards the solid state structure of ILs. Initial modeling studies focused on basic [1-methyl-3-ethylimidazolium][$AlCl_4$] systems and two models were proposed for the ionic structures; a stack model in which the anions were located between parallel planes of cations, or one in which Cl^- interacts with each hydrogen on the ring through hydrogen bonding (*49,50*). The crystal structure for [C_2mim][I] shows hydrogen bonding between the anion and the C-2 ring hydrogen (*51*).

For the [$C_n$mim][PF_6] ILs, the length of the alkyl chains and the ring substitution affects the solid state structure of the ILs. The crystal structure for [C_2mim][PF_6] has been reported (*52*) and we have obtained the crystal structure for [C_{10}mim][PF_6] (*32*). [C_{10}mim][PF_6], which melts at 38 °C and has been used in separations at elevated temperatures (*3*), has a unit cell where the cations are oriented in a bilayer arrangement. A similar arrangement has been observed for [C_{12}mim][PF_6] (*24*) where the cation structure also displays a noticeable, and yet unexplained, hook in the alkyl chain.

ILs display essentially 'salt-like' crystal packing in three dimensions for those cations containing short alkyl chains, while a restricted environment about the charged region is present in the bilayer structure for those with longer alkyl chains. The interactions are dominated by ion-ion coulombic interactions in PF_6^-

structures and change with cation size. Thus, it appears that the key to designing ILs lies in understanding weak interactions that arise in addition to the coulombic interactions. By necessity, the cations and anions will orient themselves in a salt-like manner, but it is the interactions that result from packing frustration that are noticeable in the ILs.

As shown in Figure 10, the cation structures and lattice arrangements show a trend in charged vs. non-charged separations and hydrophobic packing in the structure. The crystal structure for the cation and packing diagram for [1-butyl-2,3-dimethylimidazolium][PF_6] is shown in 10a where no distinct regions of hydrophobicity are observed, owing to the length of the alkyl chain. Adding a methyl group to the C-2 in place of a hydrogen significantly increases the melting point of this IL, considering [C_4mim][PF_6] exists as a glass under practical conditions (2). Figure 10b shows the cation and unit cell for [C_{10}mim][PF_6]. As shown in the packing diagram, the bilayer arrangement dominates the structure, leaving a charge-rich region for the cation ring and anion to interact. Figure 10c shows the cation and lattice arrangement for [C_2mim][PF_6].

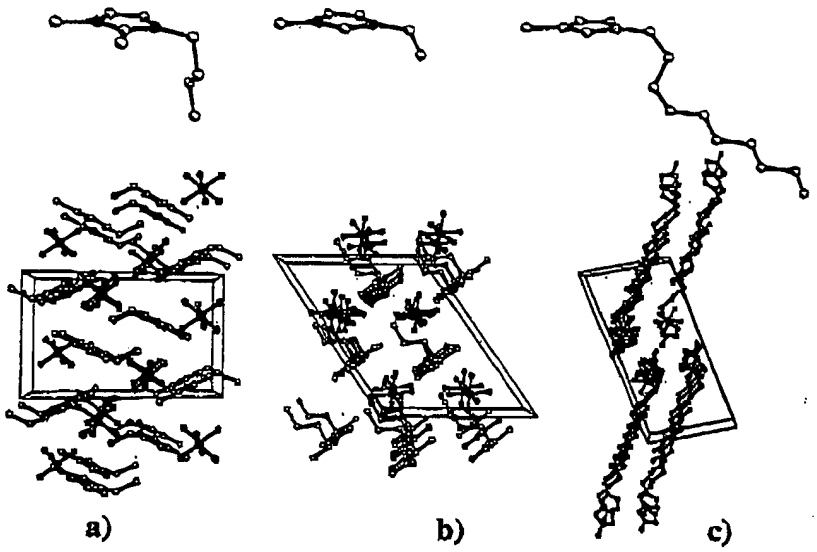

Figure 10. Cation and packing diagrams for three imidazolium-based PF_6^- ILs.

The alkyl chain length appears to have a significant influence on the solid-state structures for imidazolium-based ILs and results in two major types of orientations; salt-like and bilayer. Future solid-state analysis will facilitate the

understanding of ILs as to what cation and anion structural parameters contribute to stabilizing the resulting IL and the nature of the predominant interactions.

Conclusions

For separations, challenges lie in understanding the partitioning results with regards to those from more traditional systems. Continued study of organic solute behavior in RTIL-based liquid-liquid separations may facilitate a molecular level understanding of the partitioning mechanisms for neutral and ionic solutes, ultimately providing a predictive tool for their behavior. Exploring the driving forces for organic solute partitioning will contribute to the understanding of metal ion extractants, partitioning mechanisms in RTIL systems, and allow incorporation of new concepts such as Task Specific Ionic Liquids for separations.

Beyond the applications of ILs in liquid-liquid systems, the assortment of available and potential hydrophobic and hydrophilic RTILs attests to their easily manipulated physical properties. Through careful selection of cations and anions, significant or subtle changes can be made to the water content and rheological properties of the resulting RTILs. Indeed, crystallographic analyses indicate the structures of ILs result from several types of interactions which depend on the cation substitution and anion type.

The burgeoning field of IL research is producing exciting results and continues to demonstrate the potential for ILs in a variety of applications. Especially from the "Green Chemistry" standpoint, the chemical and physical properties of ILs, combined with their demonstrated utility as solvent replacements, warrants further study and exploration. Thus, the number of new and exciting examples of IL implementation in separations schemes is limited to time and the imagination.

Acknowledgements

Our research in this area is supported by the U. S. Environmental Protection Agency through grant number R-82825701-0. (Although the research described in this article has been funded in part by EPA, it has not been subjected to the Agency's required peer and policy review and therefore does not necessarily reflect the views of the Agency and no official endorsement should be inferred.) Additional support to the CGM by the PG Research Foundation is gratefully acknowledged.

References

1. Welton, T. *Chem. Rev.* **1999**, *99*, 2071.
2. Huddleston, J. G.; Visser, A. E.; Reichert, W. M.; Willauer, H. D.; Broker, G. A.; Rogers, R. D. *Green Chem.* **2001**, *3*, 156.
3. Visser, A. E.; Swatloski, R. P.; Rogers, R. D. *Green Chem.* **2000**, *2*, 1.
4. Visser, A. E.; Swatloski, R. P.; Reichert, W. M.; Griffin, S. T.; Rogers, R. D. *Ind. Eng. Chem. Res.* **2000**, *39*, 3596.
5. Visser, A. E.; Swatloski, R. P.; Griffin, S. T.; Hartman, D. H.; Rogers, R. D. *Sep. Sci. Technol.* **2001**, *36*, 785.
6. Visser, A. E.; Swatloski, R. P.; Reichert, W. M.; Rogers, R. D.; Mayton, R.; Sheff, S.; Wierzbicki, A.; Davis, J. H. Jr. *Chem. Commun.* **2001**, 135.
7. *Handbook of Separations Techniques for Chemical Engineers*; Schweitzer, P. A., Ed.; McGraw-Hill: New York, NY, 1996.
8. Anastas, P. T.; Warner, J. C. *Green Chemistry: Theory and Practice*; Oxford University Press: New York, NY, 1998.
9. Blanchard, L. A.; Brennecke, J. F. *Ind. Eng. Chem. Res.* **2001**, *40*, 287.
10. Cull, S. G.; Holbrey, J. D.; Vargas-Mora, V.; Seddon, K. R.; Lye, G. J. *Biotechnol. Bioeng.* **2000**, *69*, 227.
11. Dai, S.; Ju, Y. H.; Barnes, C. E. *J. Chem. Soc. Dalton Trans.* **1999**, 1201.
12. Pitner, W. R.; Rooney, D. W.; Seddon, K. R.; Thied, R. C. World Patent 99/41752, August 19, 1999.
13. Eiteman, M. A.; Gainer, J. L. *Biotechnol. Prog.* **1990**, *6*, 479.
14. Huddleston, J. G.; Lyddiatt, A. *App. Biochem. Biotech.* **1990**, *26*, 249.
15. Willauer, H. D.; Huddleston, J. G.; Griffin, S. T.; Rogers, R. D. *Sep. Sci. Technol.* **1999**, *34*, 1069.
16. Fang, Z.; Xu, S.; Kozinski, J. A. *Ind. Eng. Chem. Res.* **2000**, *39*, 4536.
17. Sasaki, M.; Fang, Z.; Fukuskima, Y.; Adschiri, T.; Arai, K. *Ind. Eng. Chem.* **2000**, *39*, 2883.
18. *Solvent-Free Polymerizations and Processes: Minimization of Conventional Organic Solvents*; Long, T. E.; Hunt, M. O., Eds.; American Chemical Society: Washington, DC, 1999.
19. Ohrenberg, C.; Geiger, W. E. *Inorg. Chem.* **2000**, *39*, 2948.
20. Furton, K. G.; Morales, R. *Anal. Chim. Acta* **1991**, *246*, 171.
21. Poole, S. K.; Shetty, P. H.; Poole, C. F. *Anal. Chim. Acta* **1989**, *218*, 241.
22. Sun, J.; Forsyth, M.; MacFarlane, D. R. *J. Phys. Chem. B* **1998**, *102*, 8858.
23. Robinson, J.; Osteryoung, R. A. *J. Am. Chem. Soc.* **1979**, *101*, 323.
24. Gordon, C. M.; Holbrey, J. D.; Kennedy, A. R.; Seddon, K. R. *J. Mater. Chem.* **1998**, *8*, 2627.
25. McFarlane, D. R.; Sun, J.; Golding, J.; Meakin, P.; Forsyth, M. *Electrochim. Acta*, **2000**, *45*, 1271.
26. Visser, A. E.; Holbrey, J. D.; Rogers, R. D. *Chem. Commun.* **2001**, 2484.

27. Bonhôte, P.; Dias, A.-P.; Papageorgiou, N.; Kalyanasundaram, K.; Grätzel, M. *Inorg. Chem.* **1996**, *35*, 1168.
28. Holbrey, J. D.; Seddon, K. R. *J. Chem. Soc. Dalton Trans.* **1999**, 2133.
29. Huddleston, J. G.; Willauer, H. D.; Swatloski, R. P.; Visser, A. E.; Rogers, R. D. *Chem. Commun.* **1998**, 1765.
30. Swatloski, R. P.; Visser, A. E.; Reichert, W. M.; Broker, G. A.; Farina, L. M.; Holbrey, J. D.; Rogers, R. D. *Chem. Commun.* **2001**, 2070.
31. Visser, A. E.; Swatloski, R. P.; Hartman, D. H.; Huddleston, J. G.; Rogers, R. D. In *Calixarenes As Ligands in Environmentally-Benign Liquid/Liquid Extraction Media*; Lumetta, G. J.; Rogers, R. D.; Gopalan, A. S., Eds.; American Chemical Society: Washington, DC, 1999; pp 223-236.
32. Rogers, R. D.; Visser, A. E.; Swatloski, R. P.; Hartman, D. H. In *Metal Ion Separation Technologies Beyond 2000: Integrating Novel Chemistry with Processing*; Liddell, K. C.; Chaiko, D. J., Eds.; The Minerals, Metals, and Materials Society: Warrendale, PA, 1999; pp 139-147.
33. Horwitz, E. P.; Muscatello, A. C.; Kalina, D. G.; Kaplan, L. *Sep. Sci. Technol.* **1981**, *16*, 1127.
34. Horwitz, E. P.; Martin, K. A.; Diamond, H.; Kaplan, L. *Solv. Extr. Ion Exch.* **1986**, *4*, 449.
35. Sachleben, R. A.; Deng, Y.; Bailey, D. R.; Moyer, B. A. *Solv. Extr. Ion Exch.* **1997**, *14*, 995.
36. Moyer, B. A.; Bonnesen, P. V. In *Physical Factors in Anion Separations*; Bianchi, A.; Bowman-James, K.; Garcia-España, E., Eds.; Wiley: New York, NY, 1997; pp 1-38.
37. Visser, A. E.; Griffin, S. T.; Hartman, D. H.; Rogers, R. D. *J. Chromatogr. B* **2000**, *743*, 107.
38. Gao, J.; Hu, G.; Kang, J.; Bai, G. *Talanta* **1993**, *40*, 195.
39. Anderson, R. G.; Nickless, G. *The Analyst* **1967**, *92*, 207.
40. Horwitz, E. P.; Dietz, M. L.; Fisher, D. E. *Solv. Extr. Ion Exch.* **1990**, *8*, 557.
41. *NIST Database 46: Critically Selected Stability Constants of Metal Complexes Database v 5.0*; U.S. Department of Commerce: Gaithersburg, MD, 1998.
42. Rogers, R. D.; Griffin, S. T. *J. Chromatogr. B* **1998**, *711*, 277.
43. Wasserscheid, P.; Keim, W. *Angew. Chem. Int. Ed.* **2000**, *39*, 3772.
44. Koch, V. R.; Nanjundiah, C.; Carlin, R. T. U. S. Patent 5,827,602, October 27, 1998.
45. Holbrey, J. D.; Seddon, K. R *J. Chem. Soc. Dalton Trans.* **1999**, 2133.
46. Seddon, K. R.; Stark, A.; Torres, M.-J. *Pure Appl. Chem.* **2001**, *72*, 2275.
47. McEwen, A. B.; Ngo, H. L.; LeCompte, K.; Goldman, J. L. *J. Electrochem. Soc.* **1999**, *146*, 1687.

48. Ngo, H. L.; LeCompte, K.; Hargens, L.; McEwen, A. B. *Thermochim. Acta* **2000**, *357-358*, 97.
49. Dieter, K. M.; Dymek, C. J.; Heimer, N. E.; Rovang, J. W.; Wilkes, J. S. *J. Am. Chem. Soc.* **1988**, *110*, 2722.
50. Dymek, C. J.; Stewart, J. P. *Inorg. Chem.* **1989**, *28*, 1472.
51. Abdul-Sada, A. K.; Greenway, A. M.; Hitchcock, P. B.; Mohammed, T. J.; Seddon, K. R.; Zora, J. A. *Chem. Commun.* **1986**, 1753.
52. Wilkes, J. S.; Zaworotko, M. J. *Chem. Commun.* **1992**, 965.

ELSEVIER

Solid State Ionics 86–88 (1996) 351–356

SOLID STATE IONICS

G1

Conductivity study on ionic liquid/polymer complexes

Masayoshi Watanabe*, Tomoo Mizumura

Department of Chemistry, Yokohama National University, 156 Tokiwadai, Hodogaya-ku, Yokohama 240, Japan

Abstract

Ternary salt mixtures, consisting of triethylmethylammonium benzoate (TEMAB), lithium acetate (LiOAc) and lithium bis(trifluoromethylsulfonyl) imide (LiTFSI), form stable molten salts at moderate temperatures at certain compositions. A typical composition of the molten salts is TEMAB/LiOAc/LiTFSI = 7/2/1 in molar ratio, and the glass transition temperature, the crystallization temperature and the melting temperature are −52°C, 30°C and 55°C, respectively. Quenched salt mixture having the above composition forms a stable supercooled liquid at room temperature, and the ionic conductivity is 10^{-4} Scm^{-1} at 30°C and 10^{-3} Scm^{-1} at 60°C. Some commercially available polymers such as polyacrylonitrile and poly(vinyl butyral) are compatible with the salt mixture to result in film forming polymer electrolytes with 1–2 order(s) of magnitude of loss of the molten salt conductivity.

Keywords: Polymer electrolyte; Molten salt; Ionic liquid; Ionic conductivity

1. Introduction

A rather new concept of addition of small amounts of polymers to real or supercooled ionic liquids has been reported [1–7] to combine high ionic conductivity and rubbery compliance in resulting polymer electrolytes. The high conductivity and rubbery compliance are due to the ionic liquids and to entanglement effects of the polymers, respectively. The concept may come from the limitation in conductivity of conventional polyether-based polymer electrolytes, where, in contrast, small amounts of salts are dissolved in the polymers, and the ionic motion is coupled with the segmental motion. The limitation is based on the inconsistency of simultaneous increases in both the number of carrier ions and their mobility, because the increase in salt concentration causes the increase in glass transition temperature (T_g) of the host polymers. We have explored [1–3] that the addition of small amounts of high molecular weight poly(1-butyl-4-vinylpyridinium halide) to room temperature molten salts, consisting of 1-butylpyridinium halide and aluminium chloride, yields new polymer electrolytes having higher ionic conductivity than 10^{-3} Scm^{-1} at room temperature and rubbery compliance.

The present work is to extend the new concept to lithium-ion-conducting polymer electrolytes. Angell et al. have recently reported [4–7] that so-called "polymer-in-salt" electrolytes, consisting of a supercooled mixture of lithium salts and a small quantity of a polymer like high molecule weight poly(ethylene oxide), give ideal polymer electrolytes for lithium battery application, because of the combination of Li^+ ion conduction and rubbery compliance. Although T_g's of the supercooled mixtures of lithium salts lie below ambient temperatures, the mixtures are thermodynamically unstable at room temperature,

*Corresponding author.

PII S0167-2738(96)00136-1

because of melting temperatures (T_m) of the mixtures being higher than room temperature [4–7]. Thus, crystallization of supercooled mixtures might be, in general, a serious drawback of Li^+ conducting polymer-in-salt electrolytes in terms of the stability of the conductivity [8]. The present study is an attempt to prepare Li^+-conducting real ionic liquids in the mixtures, consisting of triethylmethylammonium benzoate (TEMAB), lithium acetate (LiOAc) and lithium bis(trifluoromethylsulfonyl)imide (LiTFSI). Preliminary results on compatibility of the ionic liquids with some polymers and on ionic conductivity of the resulting polymer electrolytes are also presented.

2. Experimental

LiOAc (Junsei Chemical, mp: 280°C) and LiTFSI (kindly supplied by M. Gauthier of IREC, mp: 237°C) were dried under high vacuum at 180°C for 30 h before use. TEMAB (Mitsubishi Chemical) was recrystallized three times from acetone and dried under vacuum at 70°C. mp: 99°C. Polyacrylonitrile (PAN, Aldrich) and poly(vinyl butryral) (PVBu, Sekisui Chemical), which is acetalized poly(vinyl alcohol) by *n*-butylaldehyde, were dried under vacuum.

In an argon filled glove box, weighed amounts of LiOAc, LiTFSI and TEMAB were mixed in glass vials, heated to a temperature just below decomposition temperature of TEMAB, ca. 200°C, and quenched to room temperature. In the case of LiOAc/LiTFSI binary mixtures, the mixtures were heated up to a temperature, where homogeneous melts were obtained, and quenched to room temperature. To a certain composition of the ternary mixtures (TEMAB/LiOAc/LiTFSI = 7/2/1 in molar), which formed a room temperature ionic melt, PAN and PVBu were complexed in order to obtain film forming polymer electrolytes. PAN and PVBu were dissolved in N,N-dimethylformamide, and to each solution were added the molten salt to yield a homogeneous viscous solution, which was cast on a glass plate, followed by the complete evaporation of the solvent.

Ionic conductivity of both of the molten salts and the polymer electrolytes was determined by complex impedance measurements using a computer controlled HP-4192A LF impedance analyzer.

For differential scanning calorimetry (DSC) measurements of the salt mixtures, the quenched samples were sealed in Al pans in an argon filled glove box, and DSC thermograms were measured by using a Seiko Instruments DSC 220C at a heating rate of 10°C/min under nitrogen atmosphere.

3. Result and discussion

In order to realize real ionic liquids at ambient temperatures (room temperature molten salts), the phase diagram for the mixtures of LiOAc and LiTFSI was first explored. Fig. 1 shows the phase diagram for the LiOAc and LiTFSI mixtures. LiOAc is a glass forming salt, and LiTFSI is a newly developed and high dissociative salt [9]. With the addition of LiTFSI to LiOAc, T_m and T_g of the mixtures continuously decrease up to ca. 50 mol% of LiTFSI. This behaviour is similar to that observed in the lithium salt mixtures where a certain lithium salt other than LiTFSI is added to LiOAc [4]. At 50 mol% of LiTFSI, T_m and crystallization temperature (T_c) are close to 150°C, whereas T_g is 33°C. Thus, the quenched mixture behaves as a supercooled liquid at around room temperature. However, vis-

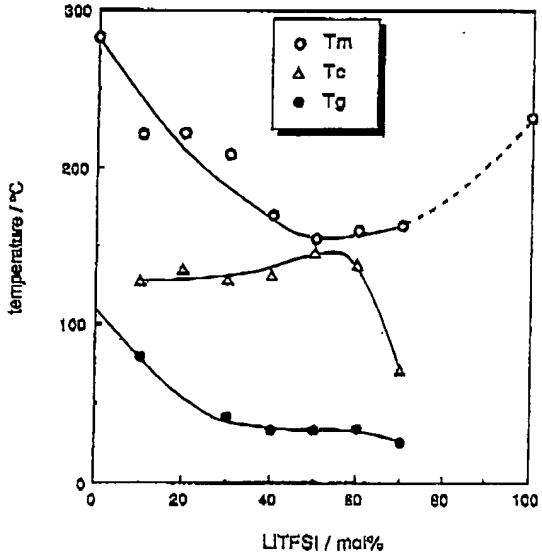

Fig. 1. Phase diagram for LiOAc and LiTFSI binary mixtures.

cosity of the mixture is quite high, and the ionic conductivity is only 10^{-6} Scm^{-1} even at 100°C. This combination was not suitable to be complexed with polymers to form polymer electrolytes.

The second strategy which we adopted to obtain stable ionic liquids is to add TEMAB to the LiOAc/LiTFSI mixtures. TEMAB has a relatively low T_m (99°C) in organic ammonium salts and aliphatic ammonium salts like TEMAB is electrochemically stable up to reduction potential of Li^+ ion. Thus, TEMAB was used to reduce T_m of the LiOAc/LiTFSI mixtures, serving as a stable ionic solvent for the mixtures. Fig. 2 shows the states of the ternary salt mixtures plotted against the compositions. Typical DSC thermograms of the salt mixtures are shown in Fig. 3, where the numerals in the thermograms correspond to the composition plots having the same numerals in Fig. 2. In Fig. 2, solid circles represent the ternary salt compositions that are inhomogeneous even at 200°C, whereas open symbols (circles, hexagons and squares) represent the compositions that form homogeneous mixtures at 200°C. The compositions represented by the open symbols can be divided into three groups, depending on the states

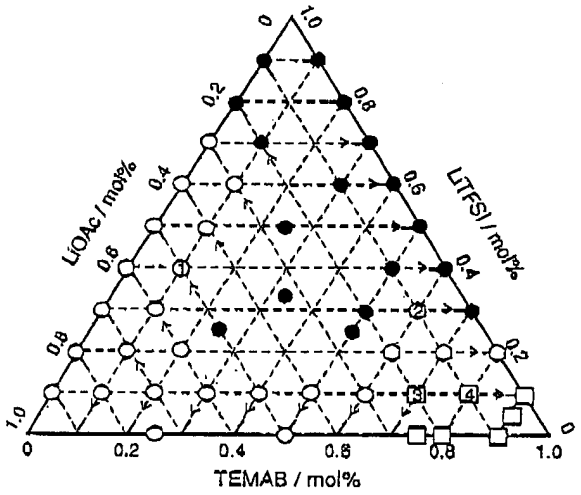

Fig. 2. States of ternary mixtures, consisting of TEMAB, LiOAc and LiTFSI, plotted against compositions: ●, inhomogeneous at 200°C; ○, homogeneous at 200°C and glassy or highly viscous at room temperature (rt) by quenching from 200°C; ⊙, homogeneous at 200°C and inhomogeneous at rt by quenching; □, homogeneous at 200°C and ionic liquids at rt by quenching. The compositions where numerals are cited in the symbols correspond to the thermograms of Fig. 3 having the same numerals.

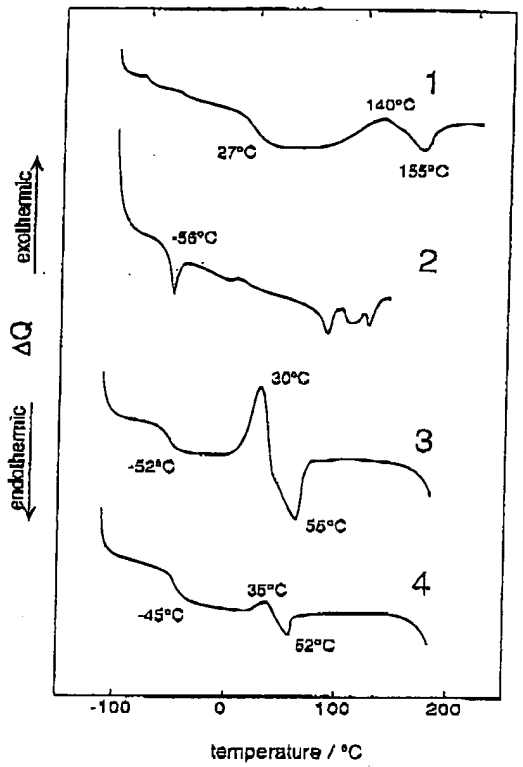

Fig. 3. DSC thermograms of typical ternary mixtures. TEMAB/LiOAc/LiTFSI: 1, 0.1/0.5/0.4; 2, 0.6/0.1/0.3; 3, 0.7/0.2/0.1; 4, 0.8/0.1/0.1.

at room temperature after quenching from 200°C. Open circles correspond to the compositions that form either glasses or highly viscous supercooled liquids at room temperature. Open hexagons correspond to the compositions that result in inhomogeneous mixtures after quenching. Ternary salt mixtures having the compositions indicated by open squares form ionic melts at room temperature by quenching. These differences are clearly reflected in the DSC thermograms shown in Fig. 3. The diagram shown in Fig. 2 reveals the following facts. The binary compatibilities between TEMAB and LiOAc and LiOAc and LiTFSI are rather good, whereas the compatibility between TEMAB and LiTFSI is poor, especially when LiTFSI composition is high. Reflecting these binary compatibilities in the ternary mixtures, homogeneous melts at 200°C (open symbols in Fig. 2) are obtained when the composition of LiTFSI is low or when the composition of TEMAB is low. For the salt mixtures having low TEMAB and high

LiOAc compositions, the quenched salts are glasses or highly viscous supercooled liquids, as seen in a typically shown DSC thermogram 1 in Fig. 3. The states of the mixtures are very close to those of the binary mixtures of LiOAc and LiTFSI, as mentioned in Fig. 1. In contrast, for the salt mixtures having high TEMAB and low LiTFSI compositions, the quenched salts form ionic melts. Typical compositions of the ionic melts are TEMAB/LiOAc/LiTFSI-7/2/1 and 8/1/1. DSC results for these two compositions are shown in the thermograms 3 and 4 of Fig. 3. T_m of the mixtures are 55°C and 52°C, respectively, and T_g's are well below room temperature. The quenched salts are found to form stable supercooled liquids at room temperature for at least a few days.

In Fig. 4 is shown temperature dependence of ionic conductivity for the salt mixture of TEMAB/LiOAc/LiTFSI = 7/2/1, abbreviated as (721) in the figure. The temperature dependence was measured with descending temperature. The salt mixture was kept at each temperature for ca. 1 h for reaching thermal equilibrium. The ionic conductivity is 10^{-4} Scm^{-1} at 30°C and 10^{-3} Scm^{-1} at 60°C. The continuously changing conductivity indicates that crystallization of the melt does not occur down to

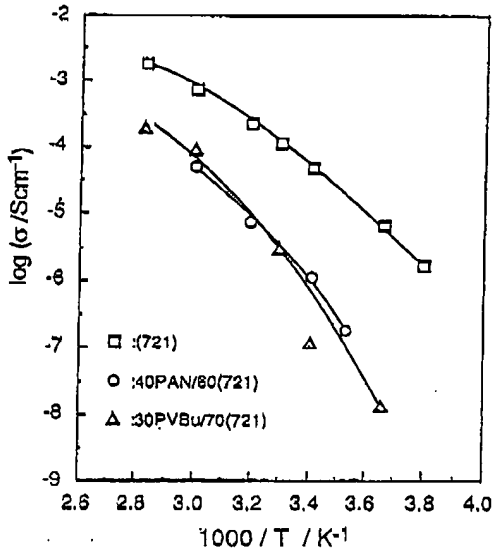

Fig. 4. Temperature dependence of ionic conductivity for ionic melt (721) (TEMAB/LiOAc/LiTFSI = 7/2/1) and its polymer complexes with polyacrylonitrile (PAN) and poly(vinyl butyral) (PVBu). The composition of the polymers are respresented in unit mol % in the figure.

− 10°C, within the time scale of measurements. The salt mixture having the composition of TEMAB/LiOAc/LiTFSI = 8/1/1 gave almost the identical conductivity with the present mixture.

Compatibility of the ionic melts with polymers has been explored by using several commercially available polymers. Up to now, PAN and PVBu give reasonable compatibility with the ionic melts. Ionic conductivity of the polymer electrolytes is shown in Fig. 4. The addition of the polymers to the ionic melts imparts film forming property to the resulting polymer electrolyte films, with a loss of 1–2 order(s) of magnitude of the molten slat conductivity. However, with standing the polymer electrolytes at room temperature for a long time, crystallization and phase separation of the salt mixtures were observed. To explore other properties than ionic conductivity, such as transport number and electrochemically stable potential-window, is currently being conducted in our group.

Acknowledgments

This research was supported in part by a Grant-in-Aid for Scientific Research on Priority Areas (No. 269/07239105) from the Japanese Ministry of Education, Science and Culture and Kanagawa Academy of Science and Technology Grants (No. 95203).

References

[1] M. Watanabe, in: Solid State Ionics: Materials and Applications, eds. B.V.R. Chowdari et al. (World Scientific, Singapore, 1992) p. 149.
[2] M. Watanabe, S. Yamada, K. Sanui and N. Ogata, J. Chem. Soc. Chem. Commun. (1993) 929.
[3] M. Watanabe, S. Yamada and N. Ogata, Electrochim. Acta 40 (1995) 2285.
[4] C.A. Angell, C. Liu and E. Sanchez, Nature 362 (1993) 137.
[5] J. Fan, R.F. Marzke and C.A. Angell, Sym. Mat. Res. Soc. 293 (1993) 87.
[6] C.A. Angell, J. Fan, C. Liu, Q. Lu, E. Sanchez and K. Xu, Solid State Ionics 69 (1994) 343.
[7] J. Fan and C.A. Angell, Electrochim. Acta 40 (1995) 2397.
[8] K. Xu and C.A. Angell, Electrochim. Acta 40 (1995) 2401.
[9] M. Armand, W. Gorecki and R. Andréani, in: 2nd Intern. Symp. Polymer Electrolytes, ed. B. Scrosati (Elsevier, London, 1990) p. 91.

J. Phys. Chem. B 2002, *106*, 12807−12813

Molecular Dynamics Study of the Ionic Liquid 1-*n*-Butyl-3-methylimidazolium Hexafluorophosphate

Timothy I. Morrow and Edward J. Maginn*

Department of Chemical Engineering, University of Notre Dame, Notre Dame, Indiana 46556

Received: August 6, 2002; In Final Form: October 4, 2002

We report the results of a molecular dynamics study of the ionic liquid 1-*n*-butyl-3-methylimidazolium hexafluorophosphate [bmim][PF_6], a widely studied ionic liquid. An all-atom force field is developed using a combination of density functional theory calculations and CHARMM 22 parameter values. Molecular dynamics simulations are carried out in the isothermal−isobaric ensemble at three different temperatures. Quantities computed include infrared frequencies, molar volumes, volume expansivities, isothermal compressibilities, self-diffusivities, cation−anion exchange rates, rotational dynamics, and radial distribution functions. Computed thermodynamic properties are in good agreement with available experimental values.

1. Introduction

The term ionic liquid (IL) has been coined in recent years to describe a class of organic salts that are liquid in their pure state at or near room temperature.[1] Some of the more widely studied ILs consist of a heterocyclic cation based on a substituted pyridine or imidazole and an inorganic anion. Early studies focused on compounds with the $[AlCl_4]^-$ anion, but these liquids proved to be unstable in air. This problem was overcome[2] through the use of alternative anions such as $[BF_4]^-$, $[NO_3]^-$, $[CH_3COO]^-$, and $[PF_6]^-$. These stable ILs have attracted a great deal of interest because of their potential as nonvolatile (and hence potentially environmentally benign) solvents.[3] They also show potential for a range of other applications including separations, industrial cleaning, fuel cells, lubricants, and heat transfer fluids.[4]

Compared to conventional organic solvents, relatively little is known about the thermodynamic and transport properties of ILs and how these properties relate to chemical constitution and structure. In addition to experimental efforts directed at this problem, a few theoretical studies have been reported in which quantum chemical[5] and classical condensed phase simulations[6−8] were used to examine structural and thermophysical properties of water-stable ILs. Other theoretical studies have focused on chloroaluminate-based ILs.[9−11]

The present work reports results of single molecule quantum chemical calculations and condensed phase classical molecular dynamics (MD) simulations on the ionic liquid 1-*n*-butyl-3-methylimidazolium hexafluorophosphate, which will be abbreviated as [bmim][PF_6]. Figure 1 shows the optimized geometry of a single [bmim][PF_6] molecule in the gas phase, obtained from a density functional theory calculation (see below). The atom labels shown in this figure will be referred to throughout the work.

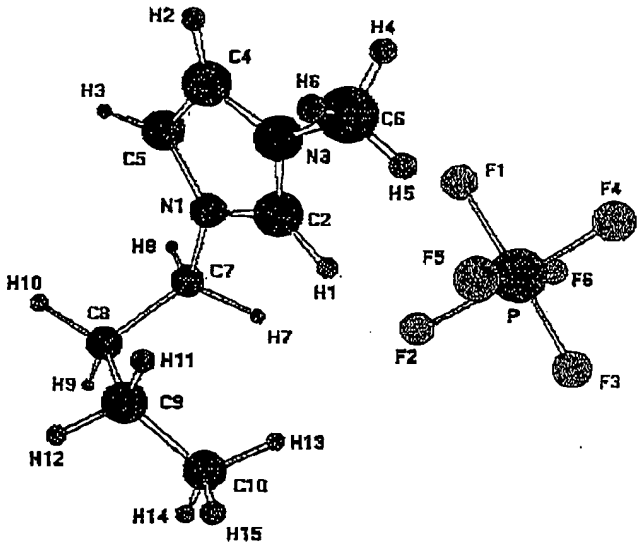

Figure 1. Geometry optimized structure of [bmim][PF_6] with atom labels noted.

2. Force Field

The extent to which a classical molecular simulation accurately predicts thermophysical properties depends on the quality of the force field used to model the interactions in the fluid. In this work, we have used a standard molecular mechanics force field,[12] with functional form

$$V_{tot} = \sum_{bonds} k_b(r - r_0)^2 + \sum_{angles} k_\theta(\theta - \theta_0)^2 + \sum_{dihedrals} k_\chi[1 + \cos(n\chi - \delta)] + \sum_{improper} k_\psi(\psi - \psi_0)^2 + \sum_{i=1}^{N-1}\sum_{j>i}^{N}\left\{\epsilon_{ij}\left[\left(\frac{r_{min,ij}}{r_{ij}}\right)^{12} - \left(\frac{r_{min,ij}}{r_{ij}}\right)^{6}\right] + \frac{q_i q_j}{r_{ij}}\right\} \quad (1)$$

where V_{tot} is the total energy of the system, harmonic potentials govern bond length, bond angle, and improper angle motion about nominal values r_o, θ_0, and ψ_0 and dihedral angles are modeled using a standard cosine series. The Lennard-Jones parameters for unlike atoms, ϵ_{ij} and $r_{min,ij}$, are obtained using the Lorentz−Berthelot combining rule. Coulombic interactions are modeled using fixed partial charges on each atom center.

* To whom correspondence should be addressed. E-mail: ed@nd.edu.

10.1021/jp0267003 CCC: $22.00
Published on Web 11/16/2002

TABLE 1: Partial Atomic Charges and Lennard-Jones Parameters Used in This Work

atom	q_i (e)	$r_{min,i}$ (Å)	ϵ_i (kJ mol^{-1})	atom	q_i (e)	$r_{min,i}$ (Å)	ϵ_i (kJ mol^{-1})
C_4	−0.141	3.600	0.209	H_9	0.055	2.680	0.117
C_5	−0.217	3.600	0.209	H_{10}	0.001	2.680	0.117
N_1	0.111	3.700	0.837	C_9	0.256	4.020	0.234
C_2	0.056	3.600	0.209	H_{11}	−0.029	2.680	0.117
N_3	0.133	3.700	0.837	H_{12}	−0.099	2.680	0.117
H_2	0.181	2.936	0.033	C_{10}	−0.209	4.080	0.326
H_3	0.207	2.936	0.033	H_{13}	0.051	2.680	0.100
H_1	0.177	1.800	0.192	H_{14}	0.040	2.680	0.100
C_6	−0.157	4.550	0.084	H_{15}	0.075	2.680	0.100
H_4	0.125	2.640	0.092	P_1	1.458	4.30	2.448
H_5	0.073	2.640	0.092	F_1	−0.421	3.400	0.377
H_6	0.142	2.640	0.092	F_2	−0.426	3.400	0.377
C_7	0.095	4.550	0.084	F_3	−0.368	3.400	0.377
H_7	0.055	2.680	0.092	F_4	−0.368	3.400	0.377
H_8	0.045	2.680	0.092	F_5	−0.364	3.400	0.377
C_8	−0.122	4.020	0.234	F_6	−0.414	3.400	0.377

With the exception of r_0, θ_0, and ψ_0 all cation intramolecular and Lennard-Jones parameters in eq 1 were taken directly from the CHARMM 22 force field[13] and used without modification. For the anion, bond length and bond angle parameters were derived from ab initio calculations, as described below. CHARMM 22 Lennard-Jones parameters were used for phosphorus and fluorine.

The minimum-energy geometry of the [bmim] cation and the [PF_6] anion was determined by performing ab initio geometry optimizations on the isolated cation and anion at the B3LYP/6-311+G* level of theory using Gaussian 98.[14] Cation and anion charges were set at +1 and −1, respectively. The resulting minimized structure was used to set r_0, θ_0, and ψ_0. Geometry optimization was also carried out on the [bmim][PF_6] pair at the same level of theory. The anion was initially located well away (over 10 Å) from the cation and facing the imidazolium C_2-carbon side. The minimum energy structure agrees very well with the results of Meng et al.[5] Partial atomic charges were derived from this geometry using the CHELPG[15] method. A listing of all force field parameters is given in Tables 1 and 2. We note that the pair calculations yielded total charges on the cation and anion of +0.904 and −0.904, respectively. In addition, the anion is slightly polarized (i.e., the charges on the fluorine atoms are not symmetric). For most of the simulations, we used these partial charges as a simple approximation of the induced polarization of the ions that occur in the liquid. This turned out not to be essential, given that the anion exhibited no preferential orientation relative to the nearest cation, as determined by monitoring the fraction of the time a given fluorine atom was closest to the C_2 carbon of the cation. We also performed simulations on an anion with symmetric charges totaling −0.904 and found essentially no difference in the computed properties.

The force constants k_b and k_θ for the anion were determined by performing a vibrational analysis on the geometry-optimized pair within Gaussian 98. The normal modes corresponding to

TABLE 2: Bond, Angle, Dihedral, and Improper Force Constants

force bonds	force constant k_b (kJ mol^{-1} Å^{-2})	r_0 (Å)	force bonds	force constant k_b (kJ mol^{-1} Å^{-2})	r_0 (Å)
C_6–N_3	220.0	1.470	C_7–$H_{7,8}$		1.091
C_7–N_1	220.0	1.483	$C_{8,9}$–$H_{9,10,11,12}$		1.096
$C_{5,4}$–$N_{1,3}$	400.0	1.382	C_{10}–$H_{13,14,15}$		1.093
C_2–$N_{1,3}$	400.0	1.337	C_7–C_8	200.0	1.530
C_4–C_5	410.0	1.361	C_8–C_9	222.5	1.534
C_2–H_1		1.078	C_9–C_{10}	222.5	1.530
$C_{4,5}$–$H_{2,3}$		1.078	P–F	260.3	1.646
C_6–$H_{4,5,6}$		1.089			

angles	k_θ (kJ mol^{-1} rad^{-2})	θ_0 (deg)	angles	k_θ (kJ mol^{-1} rad^{-2})	θ_0 (deg)
C_8–C_7–N_1	140.0	112.6	$H_{4,5,6}$–C_6–H	35.5	109.3
$C_{5,4}$–$N_{1,3}$–C_2	130.0	125.9	$H_{7,8}$–C_7–H	35.5	107.2
$H_{4,5,6}$–C_6–N_3	30.0	109.6	$H_{7,8}$–C_7–C_8	33.4	111.5
H_1–C_2–$N_{1,3}$	30.0	106.8	$H_{9,10}$–C_8–C_7	33.4	109.5
N_1–C_5–C_4	130.0	107.2	$C_{7,8}$–$C_{8,9}$–$C_{9,10}$	58.4	111.6
N_1–C_2–N_3	130.0	109.1	H–$C_{8,9}$–H	34.5	106.4
$N_{1,3}$–C_2–H_1	25.0	125.5	$C_{8,9}$–$C_{9,10}$–H	34.6	109.7
$H_{2,3}$–$C_{4,5}$–C	25.0	130.8	$H_{13,14,15}$–C_{10}–H	35.5	107.6
N_3–C_4–H_2	25.0	122.1	F–P–F	194.1	90.0

dihedral	k_χ (kJ mol^{-1})	n	δ (deg)	dihedral	k_χ (kJ mol^{-1})	n	δ (deg)
C_2–N_3–C_4–C_5	14.0	2	180	H_2–C_4–N_3–C_2	3.0	2	180
N_1–C_5–C_4–N_3	14.0	2	180	$N_{1,3}$–$C_{5,4}$–$C_{4,5}$–$H_{2,3}$	3.0	2	180
N_1–C_2–N_3–C_4	14.0	2	180	$N_{1,3}$–C_2–$N_{3,1}$–$C_{6,7}$	0.0	2	180
H_1–C_2–$N_{1,3}$–$C_{5,4}$	3.0	2	180	H_1–C_2–$N_{3,1}$–$C_{6,7}$	0.0	2	180
H_2–C_4–C_5–H_3	2.0	2	180	$H_{2,3}$–$C_{4,5}$–$N_{3,1}$–$C_{6,7}$	0.0	2	180
$C_{4,5}$–$C_{5,4}$–$N_{1,3}$–$C_{7,6}$	0.0	1	0	C_2–$N_{1,3}$–$C_{7,6}$–H	0.195	2	180

dihedral	k_χ (kJ mol^{-1})	n	δ (deg)	dihedral	k_χ (kJ mol^{-1})	n	δ (deg)
$C_{4,5}$–$N_{3,1}$–$C_{6,7}$–H	0.0	3	0	N_1–C_7–C_8–$H_{9,10}$	0.0	3	0
C_2–$N_{3,1}$–C_7–C_8	0.1	3	180	C_7–C_8–C_9–C_{10}	0.15	1	0
C_5–N_1–C_7–C_8	0.2	4	0	$H_{7,8}$–C_7–C_8–$H_{9,10}$	0.195	3	0
N_1–C_7–C_8–C_9	0.0	3	0	H_nC–C_8–C_9–H_nC	0.195	3	0
H_nC–C_9–C_{10}–H	0.16	3	0				

improper	k_ψ (kJ mol^{-1} rad^{-2})	ψ_0 (deg)	improper	k_ψ (kJ mol^{-1} rad^{-2})	ψ_0 (deg)
H_1–N_1–N_3–C_2	0.50	0	$H_{2,3}$–$N_{3,1}$–$C_{4,5}$–C	0.5	0
$N_{1,3}$–$C_{4,5}$–C_2–$C_{6,7}$	0.6	0			

the stretching of a P−F bond and the bending of an F−P−F bond were identified using Gaussview, a graphical interface for the Gaussian program, and the computed vibrational frequencies were used to calculate the corresponding harmonic force constants. The geometry and force constants for the cation and anion are summarized in Table 2. In a similar manner, vibrational assignments for the major fundamental modes of the pair were made and compared against experimental infrared spectroscopy measurements,[16,17] as described in the Results section.

3. Simulation Details

Molecular dynamics simulations of 300 [bmim] cations and 300 [PF_6] anions were performed with the program NAMD[18] version 2.4 in a cubic cell with standard periodic boundary conditions. The simulations were carried out in the isothermal−isobaric (NPT) ensemble using a Nosé-Hoover barostat to maintain a pressure of 0.98 atm. The temperature was controlled via Langevin dynamics with a damping factor of 5 ps^{-1}. Initial configurations were generated by randomly inserting cation−anion pairs into the simulation box. To prevent overlap, an insertion was rejected if any of the newly inserted atoms were within 0.75 Å of any existing atoms. The initial configurations were relaxed using a conjugant−gradient energy minimization scheme. For most of the simulations, the initial cell volume was chosen to match the experimental density of the state point of interest. All of the C−H bonds were held rigid using the SHAKE[19] algorithm. The r-RESPA[20] multiple time-stepping algorithm was used with a time step of 2 fs for bonded and van der Waals interactions and 4 fs for electrostatic interactions. The dispersion interactions were cut off beyond 20.0 Å. A switching function, initiated at a distance of 18.5 Å, was used to bring the dispersion interactions smoothly to zero at the cutoff distance. Long-range electrostatic interactions were computed using the particle mesh Ewald method.[21,22]

Prior to conducting a production run, the total energy and cell volumes were monitored until steady-state was reached. Equilibration times varied from 700 to 1000 ps, after which production runs lasting 4 ns were started. The thermodynamic properties of the system (total energy, pressure, temperature, kinetic, and potential energy contributions) were saved to disk every 100 time steps, and the atomic coordinates were saved to disk every 400 time steps. All classical simulations of [bmim]-[PF_6] were conducted at atmospheric pressure (0.98 bar) and at the temperatures 298, 323, and 343 K.

The program NAMD was chosen primarily because it is a parallel MD program that scales remarkably well with the number of processors. Simulations were run on a cluster of eight Dell Precision 530 computers running Linux. Each node contains two Intel Xeon processors operating at 1.7 GHz. A 4 ns simulation of 300 IL molecules (9600 atoms) took approximately 300 h (12.5 days) to complete.

4. Results and Discussion

Figure 2 shows the experimental[16,17] and computed IR spectra for [bmim][PF_6]. The relevant peaks in the spectra are labeled I−V. The computed frequencies of the major vibrational modes agree well with experiment. Using Gaussview, peak I was visually identified as the out-of-plane bending of the $C_2-N_1-C_5$ angle in the imidazolium ring, peak II is the F−P−F bending motion, peak III is the in-plane bending of H−C−N angles in the imidazolium ring, peak IV is the vibrational motion of several atoms in the imidazolium ring, and the peaks in region V are the stretching of C−H bonds. The computed frequency

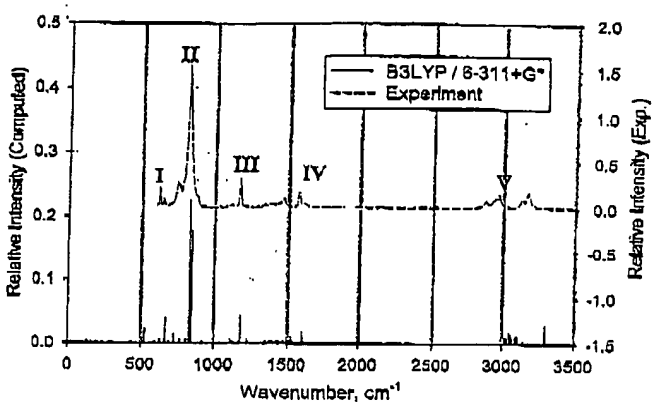

Figure 2. Comparison of computed and experimental[16] IR spectra for [bmim][PF_6].

TABLE 3: Comparison of Predicted and Experimental IR Spectral Data

assignment	pred. freq. (cm^{-1})	expt.[16] freq. (cm^{-1})
$C_2-N_1-C_5$ bend	669.9	622.9
F−P−F bend	827.5	815.8
imidazole H−C−C & H−C−N bend	1179.5	1167.7
imidazole ring bends	1600.9	1574.6
aliphatic C−H str.	3049.2	2939.1
aliphatic C−H str.	3092.9	2966.1
imidazole C−H str.	3294.8	3124.2
imidazole C−H str.	3299.3	3170.5

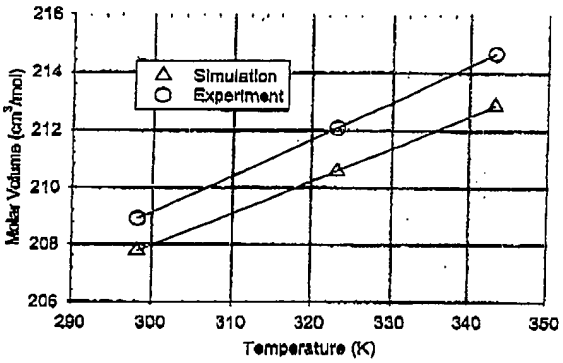

Figure 3. Comparison of predicted and experimental molar volumes of [bmim][PF_6] at 0.98 bar. Lines are linear fits to the data.

for peak I occurs at 50 cm^{-1} less than the experimental value. The agreement between computed and experimental frequencies for peaks II−IV is excellent. Peaks II and III occur at 15 cm^{-1} less than the experimental values, and peak IV occurs at 26 cm^{-1} less than the experimental value. The computed frequencies above 2800 cm^{-1} (region V) are overestimated, with errors larger than 100 cm^{-1} (see Table 3). The large errors in the predicted C−H stretching frequencies are likely due to anharmonicity effects.[23]

4.1. Molar Volume. Figure 3 shows the experimental[24] and computed molar volumes as a function of temperature at atmospheric pressure. Results are also given in Table 4. At all temperatures, the predicted molar volumes are lower than the experimental molar volumes by less than 1%. This level of agreement is excellent considering that the calculations are purely predictive; none of the force field parameters have been adjusted to match experimental data. Table 5 gives the breakdown of the potential energy into electrostatic, van der Waals, intramolecular, and kinetic energies. The average

TABLE 4: Comparison of Predicted and Experimental Molar Volumes, Volume Expansivities, and Isothermal Compressibilities at 0.98 Bar

	V (cm^3 mol^{-1})		$\alpha_P \times 10^4$ (K^{-1})		$\kappa_T \times 10^6$ (bar^{-1})	
temp (K)	sim	exp[24]	sim	exp[24]	sim	exp[24]
298.2	207.8	208.9	5.49	6.11	36.83	41.95
323.2	210.6	212.1	5.42	6.02	32.86	49.35
343.2	212.9	214.7	5.36	5.95	39.20	N/A

TABLE 5: Comparison of the Contribution of Various Terms to the System Total Energy

temp (K)	elect. (kJ/mol)	LJ (kJ/mol)	kinetic (kJ/mol)	intra. (kJ/mol)
298.2	−256.72	−89.22	100.50	89.56
323.2	−256.21	−87.19	108.92	96.74
343.2	−255.07	−85.51	116.78	102.4

electrostatic contribution to the potential energy at 298 K is −256.7 kJ/mol, which is twice as large as the van der Waals interactions and is 46 kJ/mol larger than the value reported for [emim][AlCl$_4$].[9] The total intramolecular potential energy, calculated by summing the bond, angle, dihedral, and improper angle energies, is 89.6 kJ/mol. This suggests that properties are most sensitive to the electrostatic portion of the force field.

4.2. Volume Expansivity (α_P). The volume expansivity quantifies the extent to which the volume of a fluid changes with temperature at constant pressure, and is defined as

$$\alpha_P = \frac{1}{V}\left(\frac{\partial V}{\partial T}\right)_P \tag{2}$$

The volume expansivity can be computed by running a series of simulations at the same pressure but different temperatures. Because the change of volume with temperature is approximately linear, α_P can be calculated using eq 2 by fitting a straight line to the simulated molar volume data. Table 4 lists the volume expansivities computed using this approach compared with the experimental results.[24] In all cases, the simulations predict expansivities that are lower than the experimental values by about 0.6 K^{-1}. It is observed that the predicted expansivities decrease slightly with increasing temperature, in good agreement with the experiments.

4.3. Isothermal Compressibility (κ_T). The isothermal compressibility quantifies the extent to which the volume of a fluid changes with pressure at constant temperature, and is defined as

$$\kappa_T = -\frac{1}{V}\left(\frac{\partial V}{\partial P}\right)_T \tag{3}$$

In this work, the isothermal compressibility was calculated using the following fluctuation formula[25]

$$\kappa_T = \frac{\langle \delta V^2 \rangle_{NPT}}{\langle V \rangle_{NPT} kT} \tag{4}$$

Table 4 lists the computed isothermal compressibilities compared with experimental values.[24] The computed isothermal compressibilities are consistently lower than the experimental values by 12−33%. There is still reasonably good agreement with experiment, however, especially considering the well-known difficulty in computing pressures from an atomistic simulation, as well as the inherent inaccuracy involved in computing derivative quantities using a fluctuation formula of the type in eq 4. The overall good agreement between the calculated and experimental PVT properties for this fluid indicates that the force field does a reasonable job of describing the liquid state of [bmim][PF$_6$]. The force field was therefore used to compute other thermodynamic, structural, and dynamic properties for which experimental data do not yet exist.

TABLE 6: Self-Diffusion Coefficients and Cohesive Energy Density of [bmim][PF$_6$] versus Temperature

temp (K)	$D_{[bmim]} \times 10^{-12}$ (m^2 s^{-1})	$D_{[PF_6]} \times 10^{-12}$ (m^2 s^{-1})	c (J cm^{-3})
298.2	9.70 ± 4.1	8.82 ± 4.2	761
323.2	15.4 ± 5.8	11.1 ± 5.6	738
343.2	12.1 ± 7.3	10.6 ± 7.6	727

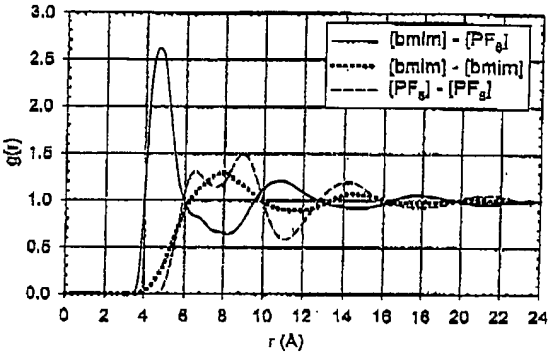

Figure 4. Center of mass radial distribution functions of [bmim][PF$_6$] at 298 K and 0.98 bar.

4.4. Cohesive Energy Density. The cohesive energy density of a liquid is defined as[26]

$$c = \frac{\Delta U^{vap}}{V^L} \tag{5}$$

where ΔU^{vap} is the change in internal energy of the liquid upon isothermal vaporization into the ideal gas state and V^L is the molar volume of the liquid. To calculate the cohesive energy density, the average internal energy and molar volume of the liquid were obtained from the liquid simulation, and the average internal energy of the ideal gas was obtained by simulating a single [bmim][PF$_6$] ion pair at the same temperature as the liquid but at zero pressure (i.e., no periodic boundary conditions). The cohesive energy density of [bmim][PF$_6$] versus temperature is given in Table 6. At 298 K, the cohesive energy density is 761 J cm^{-3}. In contrast, the cohesive energy densities of the heavy hydrocarbons hexadecane and naphthalene are 268 and 410 J cm^{-3}, respectively.[27] The extremely high cohesive energy density of [bmim][PF$_6$] stems mainly from electrostatic interactions, and explains why these liquids have such low volatility.

4.5. Molecular Structure. To obtain a better understanding of the structure of this ionic liquid, various radial distribution functions (RDFs or $g(r)$) were computed at each of the statepoints. The center-of-mass RDFs for cation−cation, cation−anion, and anion−anion pairs at 298 K and 0.98 bar are shown in Figure 4. The RDFs at 323 and 343 K are qualitatively very similar and are not shown here. It is observed that the first solvation shell for cation−anion pairs forms at about 4.3 Å. The second and third cation−anion solvation shells occur at 10.6 and 17.6 Å, respectively. Given the long-range Coulombic interactions in this system, it is not surprising to see that weak ordering persists beyond 23 Å. The first peak in the cation−cation RDF occurs at 8 Å, and the anion−anion RDF shows two peaks at 6.5 and 9 Å. This split peak is the result of sequential ordering induced by the cation−anion pairs. The RDFs agree remarkably well with those of Shah et al.,[8] who used a simpler, united atom model for this liquid.

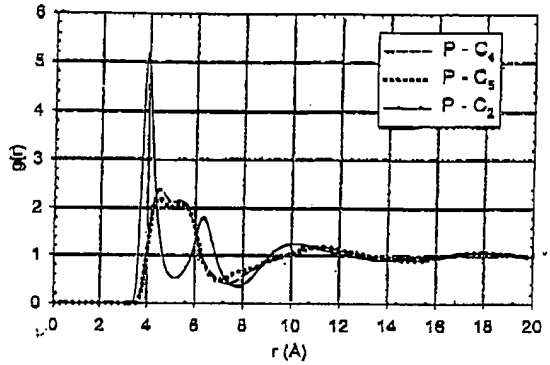

Figure 5. Atom−atom radial distribution functions for [bmim][PF_6] at 298 K and 0.98 bar.

Further insight into the liquid structure can be gained by examining the site−site pair RDFs. RDFs for the phosphorus atom of the anion and different imidazolium carbon atoms of the cation are shown in Figure 5. It is observed that the anion prefers to associate with the C_2 carbon of the imidazolium ring. The C_2−H_1 atom pair constitutes the largest amount of positive charge on the cation, so it is not surprising that the anion interacts more strongly with this part of the cation. In addition, the locations of the first peaks in the RDFs of Figure 5 are consistent with the ab initio optimized geometry of the cation−anion pair shown in Figure 1.

The RDFs suggest that the individual ions in [bmim][PF_6] tend to aggregate into well-defined ion clusters. By integrating $g(r)$ out to the location of the first minimum, the coordination number for the first solvation shell, N, can be calculated via the following equation

$$N = \int_0^{r_{shell}} \rho g(r) 4\pi r^2 \, dr \qquad (6)$$

where ρ is the bulk density and r_{shell} is the first minimum in $g(r)$. Using r_{shell} equal to 8.36 Å, the calculated coordination number for the cation−anion first solvation shell is 6.8, indicating that each ion is surrounded by a cage of nearly seven other counterions. Similarly, the cation−cation coordination number is 6.2, and the anion−anion coordination number is 6.1. Therefore, the total coordination number for the first solvation shell of an ion is nearly 13. Note, however, that the coordination numbers computed from eq 6 are sensitive to the choice of r_{shell}. For example, setting r_{shell} equal to 8.0 Å reduces the cation−anion, cation−cation, and anion−anion coordination numbers to 6.2, 5.0, and 4.9, respectively.

4.6. Diffusion. The coefficient of self-diffusion for a fluid or solid can be calculated using the Einstein relation[28]

$$D_{Self} = \frac{1}{6} \lim_{t \to \infty} \frac{d}{dt} \langle |r_i(t) - r_i(0)| \rangle \qquad (7)$$

where the quantity in braces is the ensemble-averaged mean square displacement (MSD) of the molecules and r_i is the vector coordinate of the center of mass of ion i. The mean square displacements of the cation and anion at 298 K and 0.98 bar are shown in Figure 6. The MSDs are linear up to roughly 1 ns, after which they show a slightly nonlinear increase up to about 1.8 ns, followed by a second linear regime. A block averaging technique[25] was used to obtain the MSDs, so the results are most reliable at short times. For this reason, the self-diffusion coefficients for the cation and anion were obtained by fitting the slope of the linear region from 200 to 1000 ps to a straight line and applying eq 7. Results are given in Table 6.

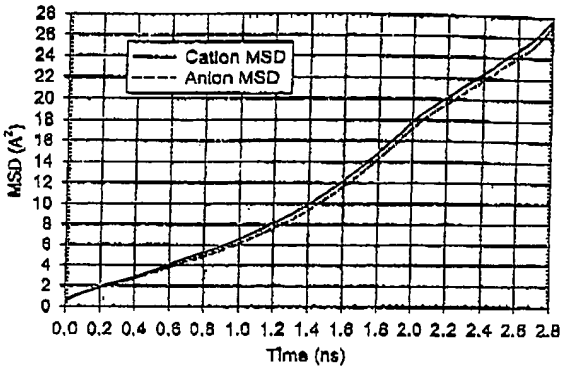

Figure 6. Center of mass mean square displacements of [bmim][PF_6] at 298 K and 0.98 bar.

At 298 K and 0.98 bar, the predicted self-diffusion coefficients of the cation and anion are 9.70×10^{-12} and 8.82×10^{-12} m^2 s^{-1}, respectively. For comparison, the self-diffusion coefficient of water[29] at 298 K and 1 atm is 2.3×10^{-9} m^2 s^{-1}. This result is consistent with the fact that [bmim][PF_6] has a much higher viscosity (450 cP)[30] than water. If one assumes that the Stokes−Einstein relation can be applied to this system, then the self-diffusion coefficients for the ionic liquid can be estimated from the relation.

$$D_{IL} = D_{H_2O} \frac{\eta_{H_2O}}{\eta_{IL}} \qquad (8)$$

where $D_{IL} = 1/2(D_{[bmim]} + D_{[PF_6]})$ and η is the viscosity. Using eq 8 and $\eta_{H_2O} = 0.9$ cP,[31] the estimated self-diffusion coefficient for the ionic liquid is 4.6×10^{-12} m^2 s^{-1}, which is fairly close to the computed value, especially considering the simplifying assumptions behind the Stokes−Einstein relation. The computed self-diffusion coefficients for [bmim] and [PF_6] are roughly 10 times smaller than those reported by de Andrade et al.,[9] who computed self-diffusivities for 1-ethyl-3-methylimidazolim ([emim]) and [$AlCl_4$] ions and are also 10 times smaller than the experimental result for [emim].[32] This is not surprising because the [emim] and [$AlCl_4$] ions are smaller than the ions in this study and because the reported intermolecular potential energy[9] for [emim][$AlCl_4$] is not as great as it is in this system. The computed self-diffusion coefficient for [PF_6] is also seven times lower than that calculated by Hanke et al.[6] from a simulation of dimethylimidazolium ([dmim]) [PF_6] at 400 K. Much of this difference could be due to the fact that the simulations of Hanke et al.[6] were at higher temperatures than the present work and because [dmim] is a smaller cation than [bmim]. We also note that the simulations in both ref 6 and 9 were over a much shorter time scale (100 ps) compared to the relatively long simulation times of this work.

The self-diffusion coefficients for [bmim] and [PF_6] could not be determined reliably by fitting the mean square displacement data at times longer than 1 ns. This was due to inaccuracies in the data caused by insufficient sampling. These inaccuracies were apparent in the relatively large (but not systematic) anisotropy in the diagonal terms of the self-diffusivity tensor at times greater than 1 ns. Long-time anisotropy in a homogeneous system indicates that even longer simulations than those in this work are needed to accurately determine MSDs above 1 ns. One must therefore leave open the possibility that the actual self-diffusivity, which by definition is a long-time quantity, may differ from that which is computed over these relatively short time scales. Nevertheless, the values reported here appear to

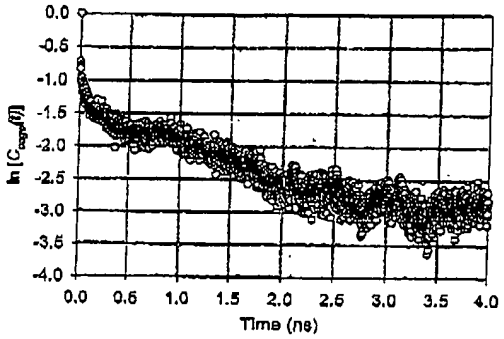

Figure 7. Time dependence of ln [$C_{cage}(t)$] for [bmim][PF_6] at 298 K and 0.98 bar.

be reasonable estimates of the actual self-diffusivity, on the basis of the semiquantitative agreement with the results obtained from the Stokes−Einstein model. The validity of the self-diffusivity can also be tested through use of the following diffusion model.

Recalling that each ion is surrounded by a cage of other ions, we hypothesize that ion diffusion involves a two-step process. In the first step, neighboring ions are displaced enough to disrupt a cage and form a diffusion pathway. In the second step, an ion leaves its cage, moving to another neighboring cage site. To test this hypothesis, the characteristic time for the breaking of ion cages was determined through use of a cage correlation function.[33] The cage for a given ion is determined by the neighbor list for that ion, defined as

$$l_i = \begin{pmatrix} f(r_{i1}) \\ \vdots \\ f(r_{iN}) \end{pmatrix} \tag{9}$$

where $f(r_{ij})$ is the Heaviside function

$$f(r_{ij}) = H(r_{cut} - r_{ij}) = \begin{cases} 1 & \text{if } r_{ij} \le r_{cut} \\ 0 & \text{otherwise} \end{cases} \tag{10}$$

and r_{cut} is a cutoff radius for the neighbor list. The cage correlation function is defined as

$$C_{cage}(t) \equiv \langle H(1 - n_i^{out}(0,t)) \rangle \tag{11}$$

where n_i^{out} is the number of ions that have left ion i's original neighbor list at time t and H is the Heaviside function. In computing the neighbor lists for all the ions, r_{cut} was set equal to the location of the first minimum of the cation/anion radial distribution function. Figure 7 shows ln $C_{cage}(t)$ for the system at 298 K. There is a rapid decay of $C_{cage}(t)$ at short times ($t <$ 0.5 ns), which is attributed to vibrational motion of ions near the boundary of a cage. After the period of initial rapid decay, $C_{cage}(t)$ plateaus and then decays exponentially after about 0.8−2.0 ns. It is interesting to note that 0.8 ns is about the same time in which a shift in the slopes of the MSDs is observed in Figure 6. By fitting an exponential function to the region from 0.8 to 2.0 ns, a time constant of 1.53 ns is obtained for the decay of the ion cages. This time constant is indicative of the average time needed for any particular ion to leave another ion's neighbor list.

To investigate the rate at which anions exit the ion cages, $C_{cage}(t)$ was computed by considering only the *anions* surrounding a given *cation*. A plot of ln $C_{cage}(t)$ at 298 K computed in this way is qualitatively similar to Figure 7 and is not shown here. The time constant obtained by fitting the intermediate region to an exponential is 3.46 ± 0.04 ns. Likewise, the rate at which cations exit the ion cages can be studied by computing ln $C_{cage}(t)$ by considering only the *cations* surrounding a given *anion*. The time constant computed for cation departure at 298 K is 3.25 ± 0.03 ns. It is not surprising to see that the time constant computed from Figure 7 is about half the time constants for cation and anion departures. This is because whenever a cation departs from an anion's neighbor list that cation simultaneously sees the anion depart from its own neighbor list. Thus, two cages decay whenever one ion moves out of another ion's cage.

The cage correlation results suggest that diffusion in ionic liquids can be modeled semiquantitatively as an activated hopping process. Each ion is assumed to reside on a three-dimensional lattice, with lattice spacings Δ given by the distance between peaks in $g(r)$. Ions execute a random walk between sites with a characteristic time τ, assumed to be equal to the time constant for cage decomposion. The self-diffusion coefficient for this model is simply[34]

$$D_{self} = \frac{\Delta^2}{6\tau} \tag{12}$$

To compute the self-diffusion coefficient for [bmim] using this model, we set Δ = 8 Å and τ = 3.25 ns. The resulting D_{self} for [bmim] is 3.28 × 10^{-11} m^2 s^{-1}. Using Δ = 8 Å and τ = 3.49 ns for [PF_6] gives a self-diffusivity of 3.08 × 10^{-11} m^2 s^{-1} These results are roughly three times higher than the computed self-diffusivities and a factor of 10 greater than that estimated from the Stokes−Einstein model. It should be expected that this simple model over predicts the self-diffusivity, because it does not account for correlated hoping motion. In the real system, it is likely that an ion that leaves a cage will frequently return to its original location, thus decreasing the overall displacement. The simplified model does not account for this but rather assumes that ions successfully thermalize in a new cage after each hop. Nevertheless, this simple model appears to capture much of the dynamics responsible for diffusion in this system.

4.7. Test of Sampling. Figure 6 shows that at 298 K the average ion moves only about 2 Å per ns of simulation time. This sluggish dynamics raises a serious concern over the level of phase space sampling in the current simulations, as well as the suitability of molecular dynamics for these calculations. As a simple test to determine if the simulations were stuck in a local potential energy minimum, three additional 300 molecule simulations were conducted for [bmim][PF_6] at 298 K. Each simulation was started from a different initial configuration and at different initial densities. Figure 8 shows the molar volumes of each of these simulations versus time. All three independent simulations converged to the same molar volume as that found from the original simulation started near the experimental density within approximately 200 ps. This indicates that, although phase space sampling is still a concern for this system, it appears that the present calculations have been run long enough to properly sample the equilibrium state of the system.

4.8. Other Dynamic Properties. The rotational dynamics of the anion were investigated by computing the cosine of the average angle θ between the vector from the P atom to the F_1 atom of an anion at time zero and time t. The decorrelation of this angle with time gives insight into the rotational motion of the anion. The rotational time constant was obtained by fitting an exponential function to long-time decay of $\langle \cos \theta \rangle$. The

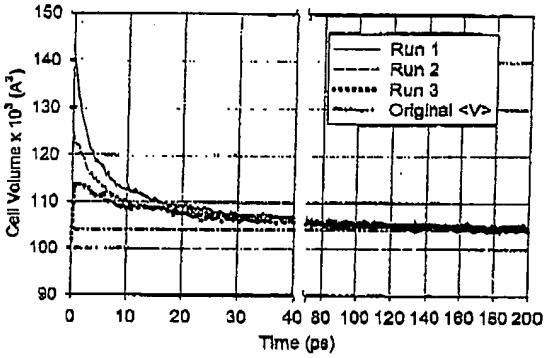

Figure 8. Plot of the cell volumes of three independent simulations of [bmim][PF6] at 298 K and 0.98 bar. The horizontal dashed line is the average volume of the original simulation.

computed time constant for anion rotation at 298 K is approximately 28.8 ps. In a similar manner, the rotational dynamics of the cation were investigated using a vector normal to the imidazolium ring. As expected, the rotational time constant is much longer at approximately 4.3 ns. This huge separation of time scales is significant; although it appears that the translational motion of cations and anions is highly correlated and slow, their rotational motions occur over vastly different time scales.

5. Conclusions

Results of a molecular dynamics simulation of [bmim][PF_6] are reported. An all-atom force field for the ionic liquid is developed using a combination of ab initio calculations and CHARMM22 parameters. The agreement between the experimental and computed IR spectra is very good, and the vibrational motions associated with various peaks in the experimental spectrum are identified. The agreement between experimental and computed values of the volume expansivity and isothermal compressibility are good, and the agreement between molar volumes is excellent. The force field was not adjusted to match the experimental data. Discrepancies between the simulation and experiment may be due to the use of unoptimized potential parameters or the neglect of polarizability. Liquid structure is reported in the form of center-of-mass radial distribution functions for cation−cation, cation−anion, and anion−anion pairs, as well as site−site RDFs. It is observed that the anion tends to orient near the C_2 carbon of the cation. Self-diffusion coefficients for [bmim] and [PF_6] are computed from the slopes of the center-of-mass mean-square displacements of the cation and anion, respectively. The reported self-diffusivities are 2 orders of magnitude smaller than the self-diffusivity of water at room temperature. The mechanism for diffusion of the ions is investigated via the computation of cage correlation functions. A simple random walk diffusion model based on this time constant yields a self-diffusivity that is in fair agreement with the calculations, as does the Stokes−Einstein estimate based on scaling with the viscosity and diffusivity of water. Rotational dynamics of the cation and anion are investigated via the computation of a common order parameter. The rotational time constants are indicative of the very slow rotational dynamics of the [bmim] cation but the relatively fast rotational motion of the [PF_6] anion.

Acknowledgment. Support for this work was provided by the National Science Foundation under Grants CTS-9987627 and DMR-0079647. We gratefully acknowledge helpful discussions with Professor Joan F. Brennecke.

References and Notes

(1) Holbrey, J. D.; Seddon, K. R. *Clean Prod. Processes* **1999**, *1*, 223.
(2) Wilkes, J. S.; Zaworotko, M. J. *J. Chem. Soc., Chem. Commun.* **1992**, 965.
(3) Welton, T. *Chem. Rev.* **1999**, *99*, 2071.
(4) Brennecke, J. F.; Maginn, E. J. *AIChE J.* **2001**, *47*, 2384.
(5) Meng, Z.; Dölle, A.; Carper, W. R. *J. Mol. Struct. (THEOCHEM)* **2002**, *585*, 119.
(6) Hanks, C. G.; Price, S. L., Lynden-Bell, R. M. *Mol. Phys.* **2001**, *99*, 801.
(7) Hanke, C. G.; Atamas, N. A.; Lynden-Bell, R. M. *Green Chem.* **2002**, *4*, 107.
(8) Shah, J. K.; Brennecke, J. F.; Maginn, E. J. *Green Chem.* **2002**, *4*, 112.
(9) de Andrade, J.; Böes, E. S.; Stassen, H. *J. Phys. Chem. B* **2002**, *106*, 3546.
(10) Takahashi, S.; Suzuya, K.; Kohara, S.; Koura, N.; Curtiss, L. A.; Saboungi, M. L. *Z Phys. Chem.* **1999**, *209*, 209.
(11) Dymek, C. J., Jr.; Stewart, J. J. P. *Inorg. Chem.* **1989**, *28*, 1472.
(12) Leach, A. R. *Molecular Modelling: Principles and Applications*, 2nd ed.; Prentice Hall: New York, 2001.
(13) MacKerell, A. D.; Bashford, D.; Bellott, M.; Dunbrack, R. L.; Evanseck, J. D.; Field, M. J.; Fisher, S.; Gao, J.; Guo, H.; Ha, S.; Joseph-McCarthy, S.; Kuchnir, L.; Kuczera, K.; Lau, F. T. K.; Mattos, C.; Michnick, S.; Ngo,, T.; Nguyen, D. T.; Prodhom, B.; Reiher, W. E., III.; Roux, B.; Schlenkrich, M.; Smith, J. C.; Stote, R.; Straub, J.; Watanabe, M.; Wiorkiewicz-Kuczera, J.; Yin, D.; Karplus, M. *J. Phys. Chem. B* **1998**, *102*, 3586.
(14) Frisch, M. J.; Trucks, G. W.; Schlegel, H. B.; Scuseria, G. E.; Robb, M. A.; Cheeseman, J. R.; Zakrzewski, V. G.; Montgomery, J. A., Jr.; Stratmann, R. E.; Burant, J. C.; Dapprich, S.; Millam, J. M.; Daniels, A. D.; Kudin, K. N.; Strain, M. C.; Farkas, O.; Tomasi, J.; Barone, V.; Cossi, M.; Cammi, R.; Mennucci, B.; Pomelli, C.; Adamo, C., Clifford, S.; Ochterski, J.; Petersson, G. A.; Ayala, P. Y.; Cui, Q.; Morokuma, K.; Malick, D. K.; Rabuck, A. D.; Raghavachari, K.; Foresman, J. B.; Cioslowski, J.; Ortiz, J. V.; Stefanov, B. B.; Liu, G.; Liashenko, A.; Piskorz, P.; Komaromi, I.; Gomperts, R.; Martin, R. L., Fox, D. J.; Keith, T.; Al-Laham, M. A.; Peng, C. Y.; Nanayakkara, A.; Gonzalez, C.; Challacombe, M.; Gill, P. M. W.; Johnson, B. G.; Chen, W.; Wong, M. W.; Andres, J. L.; Head-Gordon, M.; Replogle, E. S.; Pople, J. A. *Gaussian 98*, revision A.9; Gaussian, Inc.: Pittsburgh, PA, 1998.
(15) Brenneman, C. M.; Wiberg, K. B. *J. Comput. Chem.* **1990**, *11*, 361.
(16) Kazarian, S. IR data (personal communication).
(17) Suarez, P. A. Z.; Einloft, S.; Dullius, J. E. L.; de Souza, R. F.; DuPont, J. *J. Chim. Phys.* **1998**, *95*, 1626.
(18) Kalé, L.; Skeel, R.; Bhandarkar, M.; Brunner, R.; Gursoy, A.; Krawetz, N.; Phillips, J.; Shinozaki, A.; Varadarajan, K.; Schulten, K. *J. Comput. Phys.* **1999**, *151*, 283.
(19) Ryckaert, J. P.; Ciccotti, G.; Berendsen, H. J. C. *J. Comput. Phys.* **1977**, *23*, 327.
(20) Tuckerman, M.; Berne, B. J.; Martyna, G. J. *J. Chem. Phys.* **1992**, *97*, 1990.
(21) Darden, T. A.; York, D. M.; Pedersen, L. G. *J. Chem. Phys.* **1993**, *98*, 10089.
(22) Essmann, U.; Perera, L.; Berkowitz, M. L., Darden, T.; Lee, H.; Pedersen, L. G. *J. Chem. Phys.* **1995**, *103*, 8577.
(23) Koch, W.; Holthausen, M. C. *A Chemist's Guide to Density Functional Theory*, 2nd ed.; Wiley-VCH: New York, 2001.
(24) Gu, Z.; Brennecke, J. F. *J. Chem. Eng. Data* **2002**, *47*, 339.
(25) Allen, M. P.; Tildesley, D. J. *Computer Simulation of Liquids*; Clarendon Press: Oxford, U.K., 1987.
(26) Prausnitz, J. M.; Lichtenthaler, R. N.; de Azevedo, E. G. *Molecular Thermodynamics of Fluid Phase Equilibria*; Prentice Hall: New Jersey, 1999.
(27) Hildebrand, J. H.; Scott, R. L. *Regular Solutions*; Prentice Hall: New Jersey, 1962.
(28) Frenkel, D.; Smit, B. *Understanding Molecular Simulation*; Academic Press: New York, 1996.
(29) Hertz, H. G., Franks, F., Ed.; *Water, A comprehensive treatise*; Plenum Press: New York, 1973; Vol 3.
(30) Huddleston, J. G.; Visser, A. E.; Reichert, W. M.; Willauer, H. D.; Broker, G. A.; Rogers, R. D. *Green Chem.* **2001**, *3*, 156.
(31) Yaws, C. L.; Miller, J. W.; Shah, P. N.; Schorr, G. R.; Patel, P. M. *Chem. Eng.* **1976**, *83*, 153.
(32) Larive, C. K.; Lin, M.; Piersma, B.; Carper, W. R. *J. Phys. Chem.* **1995**, *99*, 12409.
(33) Rabani, E.; Gezelter, J. D.; Berne, B. J. *J. Chem. Phys.* **1997**, *107*, 6867.
(34) Reichl, L. E. *A Modern Course in Statistical Physics*; John Wiley & Sons: New York, 1998.